Sustainable Mesoporous Silica Nanoparticles from Groundnut Shells for High-Efficiency Cr(VI) Removal: Kinetics, Isotherms, and Mechanism Insights

Shalini, K.,[a,*] Geetha, K.,[b] Mariaamalraj, S.,[c] and Thavasilingam, K.[d]

[a]Department of Biotechnology, P.S.R. Engineering College, Sivakasi, Tamilnadu, India

[b]Department of Biotechnology, Kamaraj College of Engineering and Technology, Virudhunagar, Tamilnadu, India

[c]Department of Biotechnology, Sethu Institute of Technology, Kariapatti, Tamilnadu, India

[d]Department of Mechanical Engineering, Easwari Engineering College, Chennai, India

doi: https://doi.org/10.15255/CABEQ.2025.2450

Original scientific paper
Received: October 13, 2025
Accepted: January 7, 2026

The increasing concentrations of toxic hexavalent chromium [Cr(VI)] in aquatic systems pose a major threat to human health and the environment, necessitating the development of high-performance, reasonably priced, and environmentally friendly adsorbents. Mesoporous silica nanoparticles (SiNPs) were synthesized from groundnut shell waste via alkaline extraction followed by acid precipitation, yielding 21 %. Amorphous, mesoporous silica with a high surface area (84.61 $m^2\ g^{-1}$) and a large number of silanol groups was confirmed by characterization (XRD, FTIR, SEM–EDS, and BET). Batch adsorption experiments revealed that the maximum Cr(VI) removal efficiency reached 92 % at pH 4, with an optimum equilibrium adsorption capacity (q_e) of 4.5955 mg g^{-1}. The process followed pseudo-second-order kinetics (R^2 = 0.99) and the Freundlich isotherm model (R^2 = 0.9826), indicating chemisorption. Surface complexation was confirmed by post-adsorption analyses, demonstrating the effectiveness the SiNPs as environmentally friendly adsorbents for wastewater treatment.

Keywords

mesoporous silica nanoparticles, groundnut shell waste, hexavalent chromium removal, adsorption kinetics, chemisorption mechanism, sustainable wastewater treatment

Introduction

Heavy metals and metalloids can accumulate in terrestrial environments as a result of various activities, including the disposal of industrial wastewater, the application of fertilizers, sewage sludge, animal manure, as well as spills of petrochemicals, paints, and gasoline containing lead. To restore the affected land ecosystem, appropriate remediation techniques are required. Direct exposure to metallic pollutants through the food chain and the consumption of groundwater contaminated with heavy metals such as lead and arsenic pose significant health hazards. Ecosystems are also adversely affected when untreated effluents from the agri-food industry are discharged into river canals and other waterbodies[1]. Therefore, effective treatment methods are required to prevent heavy metal accumulation. Heavy metals can enter the human body through four primary pathways: dermal contact with contaminated sites; exposure during manufacturing, agricultural, pharmaceutical, and residential or industrial activities; inhalation from the atmosphere; and ingestion of contaminated food or water. Once ingested or inhaled, heavy metals tend to bio-accumulate in the human body and are therefore categorized as hazardous substances. Such bioaccumulation can lead to physiological and metabolic disorders. Heavy metals have been shown to affect cellular components and organelles, including cell membranes, lysosomes, enzymes, mitochondria, and nuclei. Metal ions can interact with nuclear proteins and DNA, causing DNA damage that disrupts the cell cycle and may lead to carcinogenesis or apoptosis[2].

Chromium (Cr) is one of the most hazardous heavy metals found in nature and is widely used in industrial processes. It is released from both natural sources of Cr, particularly the Earth's crust, and anthropogenic activities, primarily in trivalent [Cr(III)]

*Corresponding author: Shalini Kannan, email: shalini@psr.edu.in

and hexavalent [Cr(VI)] forms[3]. Trivalent chromium [Cr(III)] is an essential trace element for humans and other living organisms; however, both deficiency and excess can significantly affect metabolism. In contrast, Cr(VI) is highly toxic, soluble, and mobile and is considerably more harmful to humans and animals than the Cr(III) form. Numerous studies have demonstrated that inhalation of Cr(VI) increases the risk of lung cancer, with prolonged exposure in animal studies resulting in lung tumors[4]. Additionally, Cr(VI) has been shown to be toxic to invertebrates over time. Even at low concentrations, Cr(VI) can damage fish DNA, inhibit hatching, reduce lifespan, and accumulate in fish gills, subsequently affecting their internal organs such as the kidneys and liver[5,6].

Research has also indicated that Cr(VI) can cause oxidative imbalances, mutagenesis, and reductions in both above- and below-ground (root and shoot) biomass, as well as inhibit blooming, fruit setting, crop yield, and the degradation of food grain quality[7]. Silica derived from renewable sources has recently gained attention, particularly in fumed silica-reinforced bio-based wax-epoxy coatings, which have been shown to significantly improve mechanical, thermal, and moisture resistance properties[8]. Major sources of chromium pollution include chromite mining, the tannery and cement industries, asbestos degradation, emissions from catalytic converters, and organic solid waste. Chromium concentrations increase along the food chain and eventually reach humans in biomagnified form. High concentrations of chromium (Cr) are commonly detected in electroplating effluents; only 30–40 % of Cr is effectively used during electroplating, while the remainder is discharged in the final effluent, with concentrations reaching up to 1000 mg L^{-1} [9].

Current studies have focused on various methods for the removal of heavy metal ions, such as membrane technologies, advanced oxidation processes, magnetic field applications, adsorption using natural and synthetic adsorbents, and Electro Coagulation (EC)[10]. Among these methods, adsorption has attracted attention due to its low cost, high removal efficiency, operational flexibility, selectivity, and excellent stability in the removal of heavy metal ions[11,12]. Numerous studies have examined the effectiveness of low-cost adsorbents derived from agricultural waste and by-products in batch and fixed-bed sorption systems. Agricultural by-products such as groundnut shells, soybean hulls, corncobs, and rice hulls have gained significant interest as adsorbents for the treatment of contaminated wastewaters due to their abundance, low cost, and strong metal-binding capabilities[13]. Given that corn and groundnuts (peanuts) are widely consumed globally, large quantities of corncobs and groundnut shells are discarded daily into the environment. A wide range of agricultural materials, including plant seeds[14], sugarcane bagasse[15], corncob-derived biochar[16], and groundnut shell bio-char, have been explored for heavy metal adsorption[17].

Comparative studies on fumed silica-dispersed beeswax and carnauba wax epoxy coatings have shown that the morphological and dispersion characteristics of silica are the factors determining the strength of the interfacial bonding and the performance of the coatings, thus supporting the significance of tailoring silica nanostructures for specific applications[18]. Silica-based metal oxide nanoparticles possess unique properties, such as high surface area, tunable pore size, excellent bio-compatibility, and adaptable surface modification, making them effective for heavy metal adsorption. They can also alter form at different oxidation states. Additionally, these are non-toxic and environmentally safe adsorptive agents[19]. SiNPs have been successfully used to remove heavy metals from aqueous media[20]. Numerous studies have demonstrated that both unmodified SiNPs and modified SiNPs (amino-functionalized SiNPs, silica nanoparticle spheres, non-functionalized SiNPs, and amino-functionalized SiNPs gel) can effectively remove heavy metals such as Pb(II), Cd(II), Cu(II), Cr(VI), and Ni(II) from aqueous media[21].

The objective of this study was to synthesize Silica Nanoparticles (SNPs) using groundnut shells as a raw material and evaluate their performance in adsorbing hexavalent chromium ions from synthetic wastewater. Key experimental parameters affecting the adsorption process such as dosage, pH, contact time, stirring rate, and initial metal ion concentration were systematically investigated. The adsorption mechanism was analyzed through isotherm, kinetic, and thermos dynamic analyses. The synthesized SNPs showed high adsorption efficiency and good reusability for the removal of heavy metal ions from synthetic waste water. While previous studies have successfully extracted silica or silica-based adsorbents from various agricultural residues such as rice husk, corncob, and groundnut shell ash, this work presents notable advancements in synthesis efficiency, surface characteristics, and adsorption behavior. Unlike traditional methods of producing silica from rice husk requiring high temperatures and lengthy purification processes, the approach presented in this study employs groundnut shell waste and achieves approximately 21 % silica yield through a straightforward alkaline extraction-acid precipitation route. The resulting bio-silica exhibited pore structure classified as mesoporous with a relatively high specific surface area (84.61 m^2 g^{-1}), providing abundant active silanol sites for Cr(VI) adsorption. The adsorption process

closely follows a pseudo-second-order kinetic model (R^2 = 0.99), indicating chemisorption as the most important step, with performance comparable to or exceeding that of previously reported agro-waste-derived silica adsorbents. Furthermore, the total match with the Freundlich isotherm (R^2=0.9826) indicates heterogeneous and multilayer adsorption ability of the material. These combined features distinguish this study from previous reports and demonstrate the effectiveness of mesoporous silica derived from groundnut shells as a sustainable, high-performance adsorbent for Cr(VI) remediation.

Materials and methods

Analytical-grade chemicals were used throughout the study to ensure accuracy and reproducibility. Concentrated hydrochloric acid (HCl, ≥37 % purity), potassium dichromate ($K_2Cr_2O_7$, ≥99.5 % purity), sodium hydroxide pellets (NaOH, ≥98 % purity), and diphenyl carbazide (≥99 % purity) were purchased from Molychem India LLP (Mumbai, India) and used without additional purification. Distilled water, produced in-house using a double-stage glass distillation unit, was used for all solution preparations and cleaning procedures to avoid ionic interference. Groundnut shells (*Arachis hypogaea*), used as the lignocellulosic precursor, were collected from local agricultural markets in Virudhunagar, Tamil Nadu, India. The shells were washed with tap water to remove dust and adhering soil, and rinsed with filtered water to remove residual organic matter and surface contaminants.

The cleaned shells were oven-dried at 110 °C for 24 hours to remove moisture and stored in air-tight polypropylene containers until further use. All glassware was soaked overnight in 10 % nitric acid, thoroughly rinsed several times with distilled water, and dried before use to prevent contamination. Characterization was carried out using a BET surface area analyzer (Micromeritics ASAP 2020, USA), an X-ray diffractometer (Bruker D8 Advance, Germany), a scanning electron microscope coupled with energy-dispersive X-ray spectroscopy (ZEISS, Germany), and a Fourier transform infrared spectrometer (Shimadzu, Japan).

Methodology

The experimental protocol was systematically designed to synthesize mesoporous silica nanoparticles (SiNPs) from groundnut shell waste, characterize their physicochemical characteristics, and evaluate their adsorption performance for Cr(VI) removal from aqueous solutions. The workflow consisted of four main steps: (i) preparation and pretreatment of raw agricultural waste; (ii) extraction and synthesis of silica nanoparticles via alkaline solubilization and acid precipitation; (iii) physicochemical characterization using advanced analytical techniques; and (iv) batch adsorption experiments to determine the impact of process parameters, adsorption kinetics, equilibrium isotherms, and potential adsorption mechanisms. All experiments were conducted in a strictly controlled laboratory environment to ensure reproducibility and minimize external contamination. The synthesis process was adapted from established bio-silica synthesis techniques and optimized for yield, purity, and adsorption efficiency. Fourier transform infrared (FTIR) spectra were recorded over the range of 400–4000 cm^{-1} using a Shimadzu IRSpirit spectrometer. X-ray Diffraction (XRD) patterns were obtained using a PANalytical X'Pert PRO diffractometer with Cu Kα radiation (λ = 1.5406 Å). Surface morphology and elemental composition were analyzed using a Zeiss EVO18 scanning electron microscope (SEM) equipped with energy-dispersive X-ray spectroscopy (EDS). Nitrogen adsorption-desorption isotherms were measured using a Micromeritics ASAP 2020 analyzer to determine specific surface area and pore characteristics. Cr(VI) concentrations were quantified using the diphenylcarbazide method at 540 nm with a Shimadzu UV-2600 UV-visible spectrophotometer.

Synthesis of silica nanoparticles, preparation of Cr(VI) solutions, and material characterization

Groundnut shells were collected and dried at 110 °C for 24 hours. The dried groundnut shells were then combusted at 650 °C for five hours to remove volatile gases CO and CO_2, producing ash powder. Acid pretreatment was employed to enhance the purity of the silica product, as it is an effective method for producing pure white silica ash while removing most metallic impurities. Silica powder was synthesized via a dissolution-precipitation process. One gram of ash powder was mixed with 60 mL of 1 M NaOH aqueous solution. After three hours of agitation and continuous heating at 80 °C, the mixture was filtered through Whatman filter paper to dissolve the silica and produce sodium silicate (Na_2SiO_3). Gel formation was induced by adjusting the pH of the solution to 7.0 using 5 M HCl under continuous stirring, followed by incubation for 8–12 hours. The gel was subsequently washed several times and centrifuged at 4000 rpm for 5 min. After removing the supernatant, the resulting gel was dried at 80 °C for 24 hours to obtain the as-prepared xerogel, and was ground into a fine powder using a mortar and pestle[22].

The silica yield for each of the treated residues was calculated using the following equation:

$$Y = W_{Si}/W_T \cdot 100 \quad (1)$$

where Y is the yield (%), W_{Si} is the weight of obtained silica (g), W_T is the total weight of processed residue (g).

A 1000 mg L^{-1} of Cr(VI) stock solution was prepared by dissolving 2.8 g of potassium dichromate ($K_2Cr_2O_7$ analytical grade, ≥99.5 % purity) in 1 L of distilled water. The solution was stored in an amber glass bottle at room temperature (25 ± 2 °C) to prevent photo degradation. Working solutions (5–50 mg L^{-1}) were freshly prepared by serial dilution with distilled water. Solution pH (2–9) was adjusted using 0.1 M NaOH or 0.1 M NaOH and measured using a calibrated pH meter (0.01 accuracy). All glassware was acid-washed and thoroughly rinsed before use to prevent contamination. The physicochemical characteristics of the synthesized silica were characterized using advanced analytical techniques. Surface morphology and elemental composition were examined using EDS coupled with scanning electron microscopy (SEM) (ZEISS, Germany). Functional groups were identified by FTIR (Shimadzu, Japan) over the range of 400–4000 cm^{-1} at a resolution of 1 cm^{-1}. Crystallinity and phase composition were analyzed by XRD using Cu Kα radiation (λ = 1.5401 Å), with a scan rate of 1° min^{-1} at 40 kV and 40 mA. Textural parameters such as pore volume, average pore size, and specific surface area, were determined using Brunauer–Emmett–Teller (BET) and Barrett–Joyner–Halenda (BJH) techniques with a Micromeritics ASAP 2020 analyzer. All measurements were conducted under strictly controlled laboratory conditions to ensure reproducibility[23].

Adsorption experiments

The synthesized silica nanoparticles derived from groundnut shells were used as adsorbents in batch adsorption experiments for the removal of hexavalent chromium ions. All experiments were conducted in triplicate to ensure reproducibility. The effects of various operational parameters, including initial chromium concentration (5–50 mg L^{-1}), initial pH (2–8), agitation time (0–180 minutes), initial metal ion concentration (10–70 mg L^{-1}), and adsorbent dosage (0.2–2 %), were systematically investigated to determine optimal adsorption conditions.

Effect of initial chromium concentration

A dosage of 1 g L^{-1} of synthetic silica nanoparticles was added to 100 mL of aqueous solutions containing varying chromium concentrations (5–50 mg L^{-1}, intervals of 5 mg L^{-1}). Adsorption experiments were conducted at room temperature with a neutral solution pH maintained at 7± 0.05 using dilute HCl or NaOH solutions. The mixtures were agitated at 120 rpm for 180 min. After equilibration, samples were centrifuged at 6000 rpm for 10 min, and the supernatants were analyzed at 540 nm using a Shimadzu UV-2600 spectrophotometer. The Cr(VI) concentrations were determined using the standard Diphenylcarbazide (DPC) spectrophotometric method[24]. A DPC stock solution was prepared by dissolving 50 mg of DPC in 25 mL of acetone containing 250 µL of 1 N sulfuric acid. For measurement, the pH of the supernatant was adjusted to approximately 2.0 using dilute hydrochloric acid, as required for the formation of the Cr(VI)–DPC complex. Aliquots (3 mL) of the working solution were treated with 100 µL of the DPC reagent to obtain the colored Cr(VI)–DPC complex. The absorbance of the resulting colored complex was measured at 540 nm using a UV–visible spectrophotometer. The Cr(VI) concentrations were calculated using a calibration curve prepared from working standards. Percentage removal and equilibrium adsorption capacity (q_e) were calculated from the initial and residual chromium concentrations.

Effect of pH

To examine the effect of pH, 10 mg $L^{-1}$of Cr(VI) solutions containing 1 g L^{-1} SiNPs were agitated at 120 rpm for 30 minutes over a pH range of 2–8. Following pH adjustments using 0.1 N HCl or NaOH, the solutions were centrifuged and analyzed using the DPC spectrophotometric assay at 540 nm to determine removal percentage.

Effect of time

Time-dependent adsorption was investigated by agitating 1 g L^{-1} SiNPs in 10 mg L^{-1} Cr(VI) solution at pH 4 and 120 rpm. Samples were collected at intervals between 30 and 180 minutes and analyzed spectrophotometrically at 540 nm using the DPC assay. The percentage of removal was then recorded.

Effect of adsorbent dosage

To assess the effect of adsorbent dosage, SiNP dosages ranging from 0.2 to 1.6 g were added to 100 mL of 10 mg L^{-1} chromium solution. The solution was centrifuged, agitated at 120 rpm for 90 minutes while maintaining pH 4, and then spectrophotometrically examined at 540 nm using the DPC assay. The percentage removal was then calculated.

Effect of metal ion concentration

To examine the impact of different initial metal ion concentrations (10–70 mg L^{-1}) on adsorption efficiency, spectrophotometric analysis was conducted using 1 g L^{-1} SiNPs at fixed pH (4) and agitation (120 rpm for 90 min).

Batch adsorption studies: Langmuir, Freundlich, and Temkin isotherms

Equilibrium isotherm experiments were conducted using initial chromium concentrations (10–70 mg L^{-1}). The solutions were agitated at 120 rpm with 1 g L^{-1} silica nanoparticles at pH 4 for 90 min using a shaker incubator. Data were fitted to Temkin, Freundlich, and Langmuir isotherm models to quantify interactions and elucidate adsorption mechanisms.

The equilibrium adsorption capacity of groundnut silica ash for Cr(VI) (q_e, mg g^{-1}) and the removal efficiency (RE/%) were calculated using the following equations[25,26].

$$q_e\,(\text{mg g}^{-1}) = \frac{(C_i - C_e)}{W}\cdot V \tag{2}$$

$$\text{RE}\ (\%) = \frac{C_i - C_e}{C_i}\cdot 100 \tag{3}$$

where: W (g) is the amount of adsorbent (SNPs), V (L) is the volume of working solution, and C_i and C_e are the initial concentration and equilibrium concentration (mg L^{-1}) of heavy metal ions, respectively.

Statistical analysis and model validation

To ensure consistency and reproducibility, all adsorption datasets derived from the batch experiments underwent comprehensive statistical analysis. To avoid distortions associated with linear transformations, the kinetic profiles were examined using nonlinear regression to fit pseudo-first-order, pseudo-second-order, and Elovich models. Model ranking was performed using the Akaike Information Criterion (AIC) and Akaike weights to identify the most probable representation of the underlying adsorption mechanism. Model goodness of fit was assessed using the adjusted coefficient of determination (R^2 adj), Root Mean Square Error (RMSE), chi-square (χ^2), and the corrected Akaike Information Criterion (AIC).

The RMSE and χ^2 were calculated using the following equations:

$$\text{RMSE} = \sqrt{\frac{1}{n}\sum_{i=1}^{n}(q_{e,\text{exp}} - q_{e,\text{pred}})} \tag{4}$$

$$\chi^2 = \frac{\sum_{i=1}^{n}(q_{e,\text{exp}} - q_{e,\text{pred}})^2}{q_{e,\text{pred}}} \tag{5}$$

Similarly, a wide range of isotherm models, including Langmuir, Freundlich, Temkin, were fitted to equilibrium adsorption data using nonlinear optimization to estimate parameters like adsorption intensity (n), affinity constants (K_L, K_F), and maximum adsorption capacity (Q_m). Ninety-five percent confidence intervals were obtained using a parametric bootstrap approach with 2000 iterations to enable accurate parameter estimation while accounting for experimental variability. Furthermore, Welch's analysis of variance and Dunnett's post-hoc test were applied to statistically analyze optimization experiments involving pH, contact time, and adsorbent dosage. Effect sizes (Hedges' g) and achieved power were reported to supplement p-values. All analyses were conducted at a significance level of $p < 0.05$. This integrated statistical framework ensured that the conclusions drawn from the kinetic, equilibrium, and optimization studies were supported by validated models and explicit uncertainty quantification, while maintaining continuity with subsequent results, as shown in Fig. 1.

Result and discussion

Synthesis and characterization of silica particles

Silica was recovered from the groundnut shell ash through alkaline extraction followed by acid precipitation. The ash was obtained by calcining the shells at 650 °C and subsequently subjecting them to acid precipitation. A yield of 21 % based on the initial ash weight was obtained from the procedure, which produced 0.21 grams of silica from an initial mass of 1 gram of groundnut shell ash. After drying and grinding, the resulting white silica powder was homogeneous and free-flowing, indicating that contaminants had been successfully removed and that the amorphous silica had been successfully recovered from the agricultural waste feedstock.

FTIR characterization

FTIR spectroscopy was employed to examine the bonding structures and functional groups of the synthesized silica nanoparticles. The FTIR spectra (Fig. 2a and 2b) confirmed the effectiveness of silica extraction from groundnut shell ash, revealing the distinctive vibrational bands associated with silica. FTIR analysis was conducted before and after chromium adsorption onto the synthesized silica to assess potential changes in surface functional groups.

Strong Si–O–Si asymmetric stretching vibrations were observed at approximately 1138–1141 cm^{-1} along with distinct bands near 580 cm^{-1} and 440 cm^{-1}, corresponding to Si–O–Si symmetric stretching and Si–O bending, respectively. These features confirm the presence of silica in the groundnut shells. After chromium adsorption, these characteristics persisted, suggesting that the silica network structure remained intact. However, subtle changes were observed, including alterations near

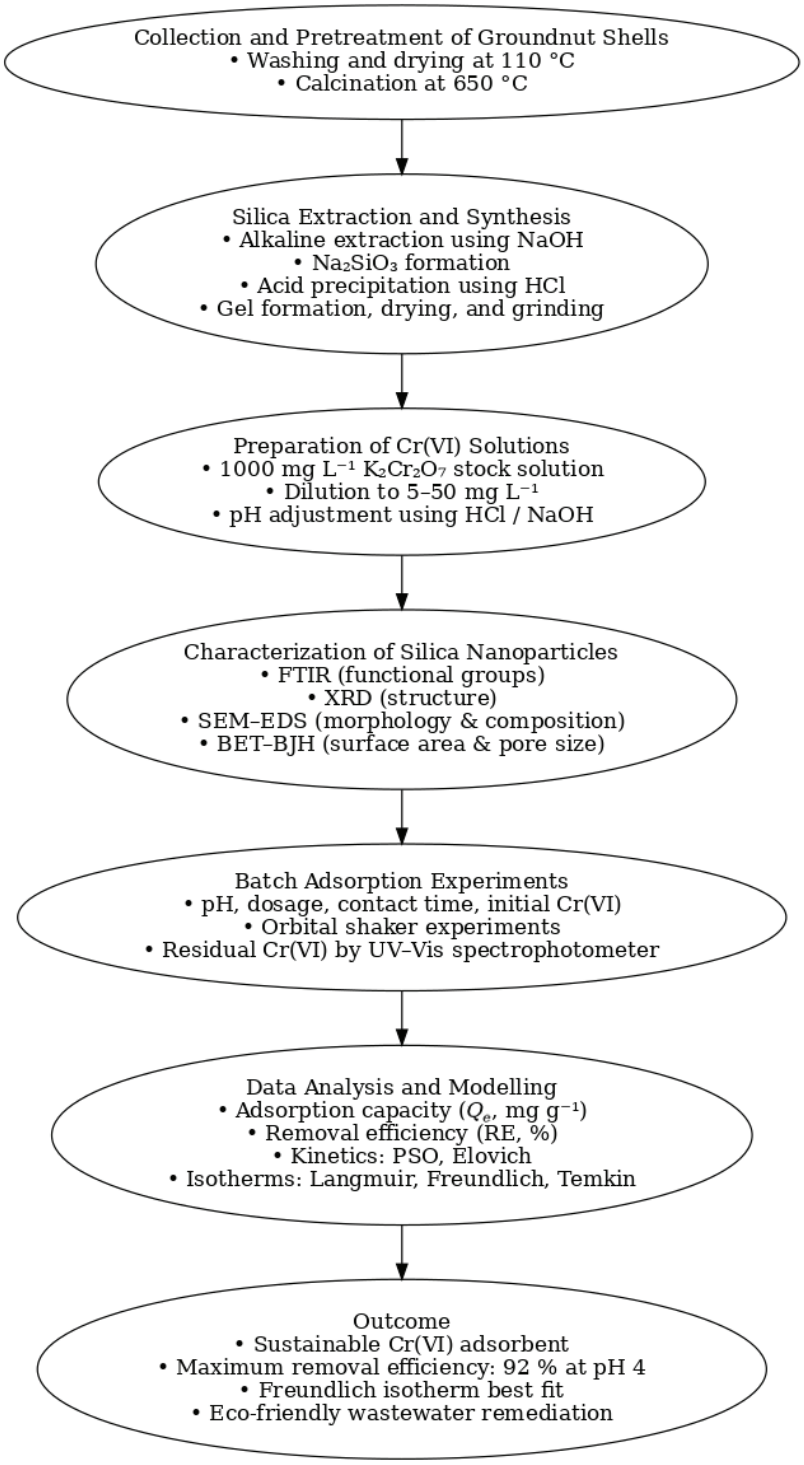

Fig. 1 – *Flowchart of the experimental methodology adopted for the synthesis, characterization, and Cr(VI) adsorption studies using mesoporous silica nanoparticles derived from groundnut shell waste*

980 cm^{-1} and a slight shift and broadening of the O–H stretching region (about 3400 cm^{-1}), suggesting interactions between the surface silanol (Si–OH) groups and chromium ions. Chromium was adsorbed onto the silica via binding through surface hydroxyl functionalities, as further supported by the reduction of isolated free –OH groups, evidenced by the diminished peak at 3609 cm^{-1} after adsorption.

The presence of silica (SiO_2) in the biomass was confirmed by distinct bands in the FTIR spectra of both the chromium-adsorbed sample (GN Absorbed) and the untreated groundnut shells (GNS). In both cases, a prominent absorption peak between 1138 and 1141 cm^{-1} corresponds to Si–O–Si asymmetric stretching vibrations, a defining feature of silica materials[27]. Additional supporting bands at

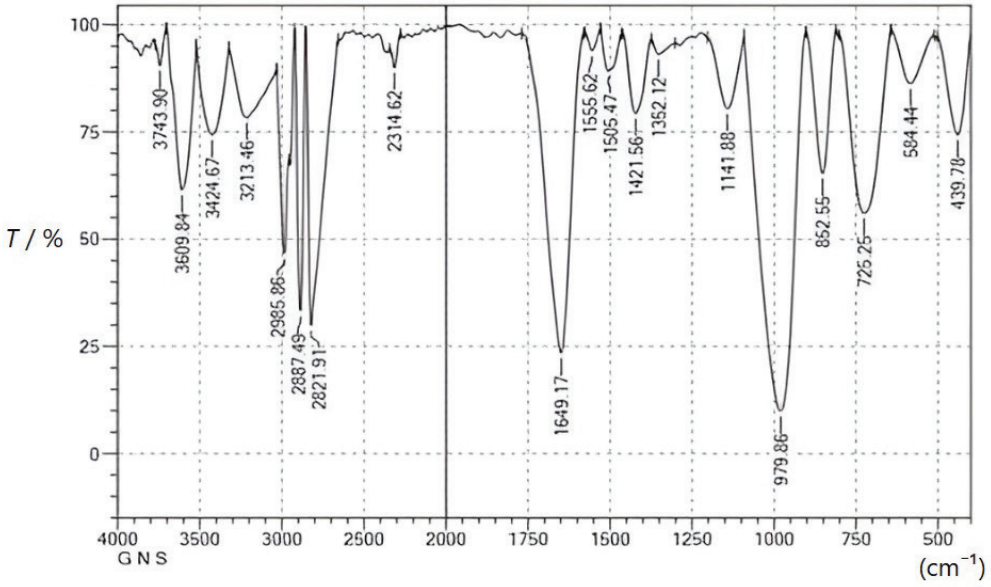

Fig. 2a – *FTIR analysis of groundnut shell silica*

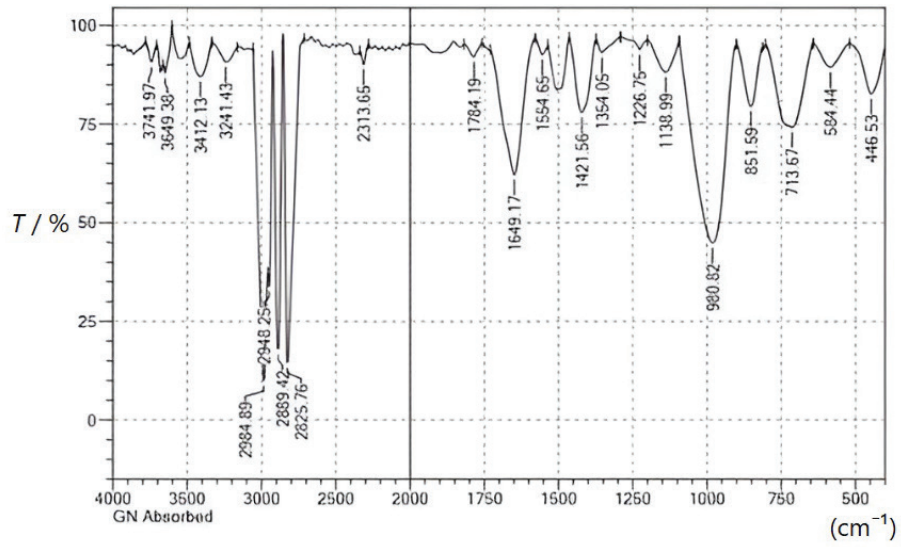

Fig. 2b – *FTIR analysis of adsorbed groundnut shell silica*

approximately 580–590 cm^{-1} and 440–450 cm^{-1} arise from Si–O–Si symmetric stretching and Si–O bending vibrations, respectively. The occurrence of these peaks in both the untreated and treated samples indicates that silica is a naturally occurring component of the groundnut shell matrix and contributes to its mechanical structure. Compared with GNS (Groundnut Shell Silica), the O–H band in chromium-adsorbed GNS appeared somewhat broadened and shifted[28], indicating interactions between hydroxyl groups on the biomass and chromium species, most likely via coordination or hydrogen bonding. After chromium adsorption, the bending vibration of water molecules or surface hydroxyl groups (~1649 cm^{-1}) became more intense, suggesting enhanced water retention or Cr interaction with surface functional groups. The peak at approximately 980 cm^{-1} was more pronounced after chromium treatment. The concept that chromium binds to groups that contain oxygen on the biomass surface was supported by the possibility that this is associated with Cr–O stretching vibrations[29]. The weak absorption bands in the 2920–2850 cm^{-1} region may be assigned to residual aliphatic C–H stretching vibrations, likely originating from trace carbonaceous residues or organic moieties remain-

ing after calcination and acid treatment, as typically reported for silica obtained from agricultural waste. The low intensity of these bands indicates that most of the organic material was effectively removed during thermal processing.

XRD patterns of groundnut shell-derived silica nanoparticles

The structural characteristics of groundnut shell-derived silica (GNS) before and after chromium adsorption were analyzed through XRD, as shown in Fig. 3. The XRD pattern of untreated bio-silica exhibited a broad diffraction hump located in the $2\theta \approx 25–30°$ range, indicative of amorphicity[28], with no sharp crystalline peaks observed. After chromium adsorption, the XRD pattern remained largely unchanged, with the amorphous hump appearing at an almost identical 2θ position and displaying a similar width and profile. No peak sharpening, shifts, or new crystalline reflections

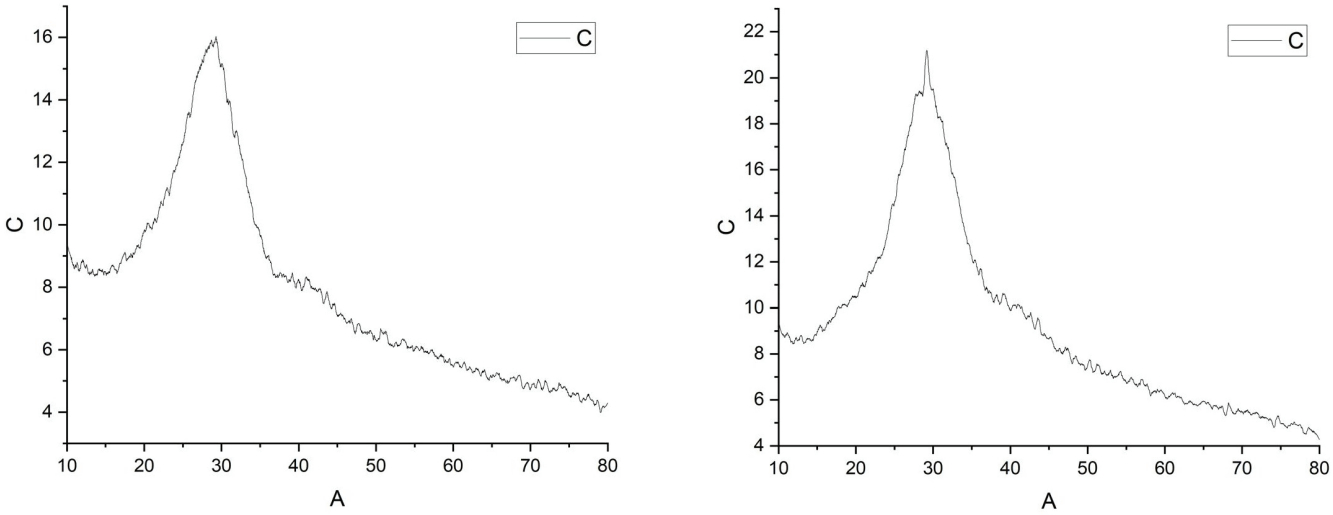

Fig. 3 – *XRD patterns of groundnut shell—derived silica nanoparticles before and after Cr(VI) adsorption*

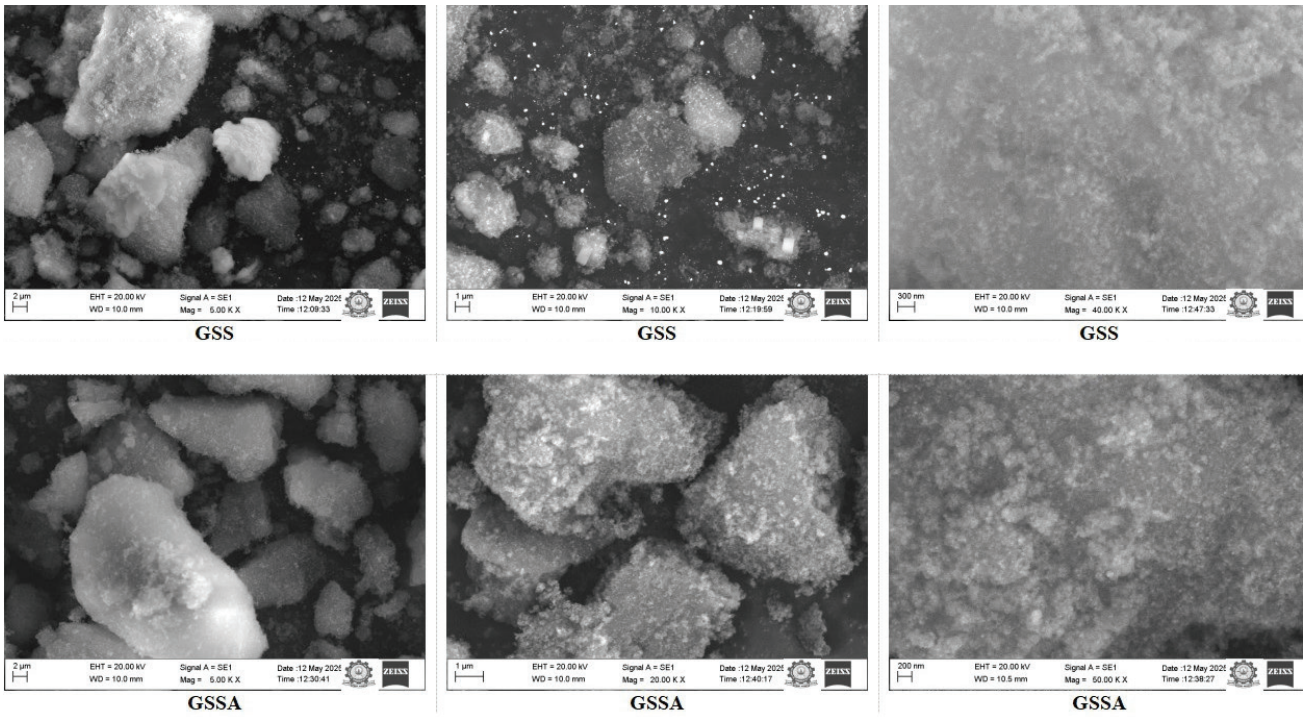

Fig. 4 – *SEM micrographs of groundnut shell-derived silica nanoparticles before and after Cr(VI) adsorption*

attributable to chromium-containing phases were detected, indicating that the silica matrix retained its structural integrity after adsorption of chromium. The slight differences in peak heights are attributed to surface coverage or sample packing effects rather than changes in the bulk structure. These findings suggest that chromium species were predominantly adsorbed onto the surface or within the pores of the amorphous silica, consistent with previous reports on bio-silica based adsorbents[30].

SEM characterization

Scanning Electron Microscopy (SEM) revealed significant morphological changes in the groundnut shell-derived silica after chromium adsorption. The SEM images (Fig. 4) of the groundnut-derived silica revealed irregularly shaped particles[31] with a rough, granular texture and no well-defined symmetry, corroborating the amorphous nature inferred from XRD analysis. The rough, porous surface shape[32] of the unmodified bio-silica indicated a large surface area conducive to adsorption. Images taken after adsorption revealed a smoother, denser surface with much less porosity. Furthermore, the development of evenly spaced, luminous nanoparticles further indicated the adsorption of chromium species. These morphological changes confirmed the effective adsorption of Cr(VI), likely facilitated by pore diffusion and surface complexation, supporting the suitability of bio-silica as an economical and effective adsorbent for heavy metal removal from aqueous solutions.

EDS analysis revealed elemental weight percentages of 27 %, 25 %, and 20 % for Si, O, and Al, respectively. Elemental mapping images of the synthesized groundnut shell silica are displayed in Fig. 5. The presence of Si was confirmed by the elemental distribution[31]. This homogeneity facilitates efficient surface interaction sites for GS-SiNPs metal adsorption onto water contaminants.

BET analysis

An adsorbent's adsorption capability is mostly determined by its porosity and pore size[32]. For the synthesized non-adsorbed groundnut shell silica (sample D) and the chromium adsorbed groundnut shell silica (sample C), the specific surface area based on the BET method, mean pore size (RBJH) based on the BJH method, and total pore volume (V_{tot}) were assessed.

The adsorption capacity of groundnut-derived silica was methodically assessed for its efficacy in the removal of chromium from aqueous solutions. Sample C exhibited a narrower H3/H4-type loop, indicating partial blockage of slit-shaped pores after chromium adsorption. Nitrogen adsorption–desorption isotherms for Sample D (Fig. 6) exhibited type IV behavior with H_2 hysteresis, typical of mesoporous materials[33] with adhesion technology[34]. Chromium interaction with the silica surface was confirmed by BET surface area analysis, which showed a significant decrease in surface area from 84.61 $m^2\ g^{-1}$ (Sample D) to 46.39 $m^2\ g^{-1}$ (Sample C) after adsorption. BJH desorption data showed corresponding reductions in average pore width (17.17 nm to 12.78 nm) and pore volume (dropped from 0.369 cc g^{-1} to 0.309 cc g^{-1}), suggesting pore filling or narrowing due to chromium retention. The mesoporous morphology of the bio-silica was validated by t-Plot analysis, which revealed minimal micro porosity (0.005 cc g^{-1}) in Sample D and a dominant exterior surface area of 73.34 $m^2\ g^{-1}$. Collectively, these results confirm that groundnut silica possesses a mesoporous structure that is ideal for adsorption, and the post-treatment decrease in textural characteristics confirms its effectiveness in chromium sequestration.

Optimization of parameters

Effect of pH

The adsorption efficiency of Cr(VI) onto groundnut shell-derived silica was found to be strongly influenced by the pH of the aqueous solution. Adsorption experiments were conducted by varying the pH from 2 to 8, using a fixed Cr(VI) initial concentration of 10 mg L^{-1}. For each test, 0.1 g of synthesized silica was added to 10 mL of the chromium solution and agitated at 180 rpm for 90 minutes at room temperature. Chromium primarily exists as $HCrO_4^-$ and $Cr_2O_7^{2-}$ under acidic conditions, while CrO_4^{2-} dominates in neutral to alkaline pH. The adsorption efficiency increased from 43.85 % at pH 2 to a peak of 92 % at pH 4. The highest removal efficiency was observed at pH 4, suggesting favorable interactions between the negatively charged Cr(VI) species and the protonated surface groups of the silica. This was likely due to the increased electrostatic attraction under acidic conditions, where the bio-sorbent surface became positively charged. However, at very low pH (pH 2), excess H^+ ions may compete with chromium anions for active sites, reducing the efficiency. Beyond pH 5, the efficiency gradually decreased, with 68.79 % removal observed at pH 8. This decline at higher pH levels can be attributed to the deprotonation of surface functional groups, which reduces electrostatic attraction to the anionic chromium species[35].

Welch's one-way ANOVA was applied to analyze the percentage removal values calculated from repeated OD measurements at pH 2–8 (control set to pH 4) to determine statistical differences across pH levels. The omnibus test revealed a significant

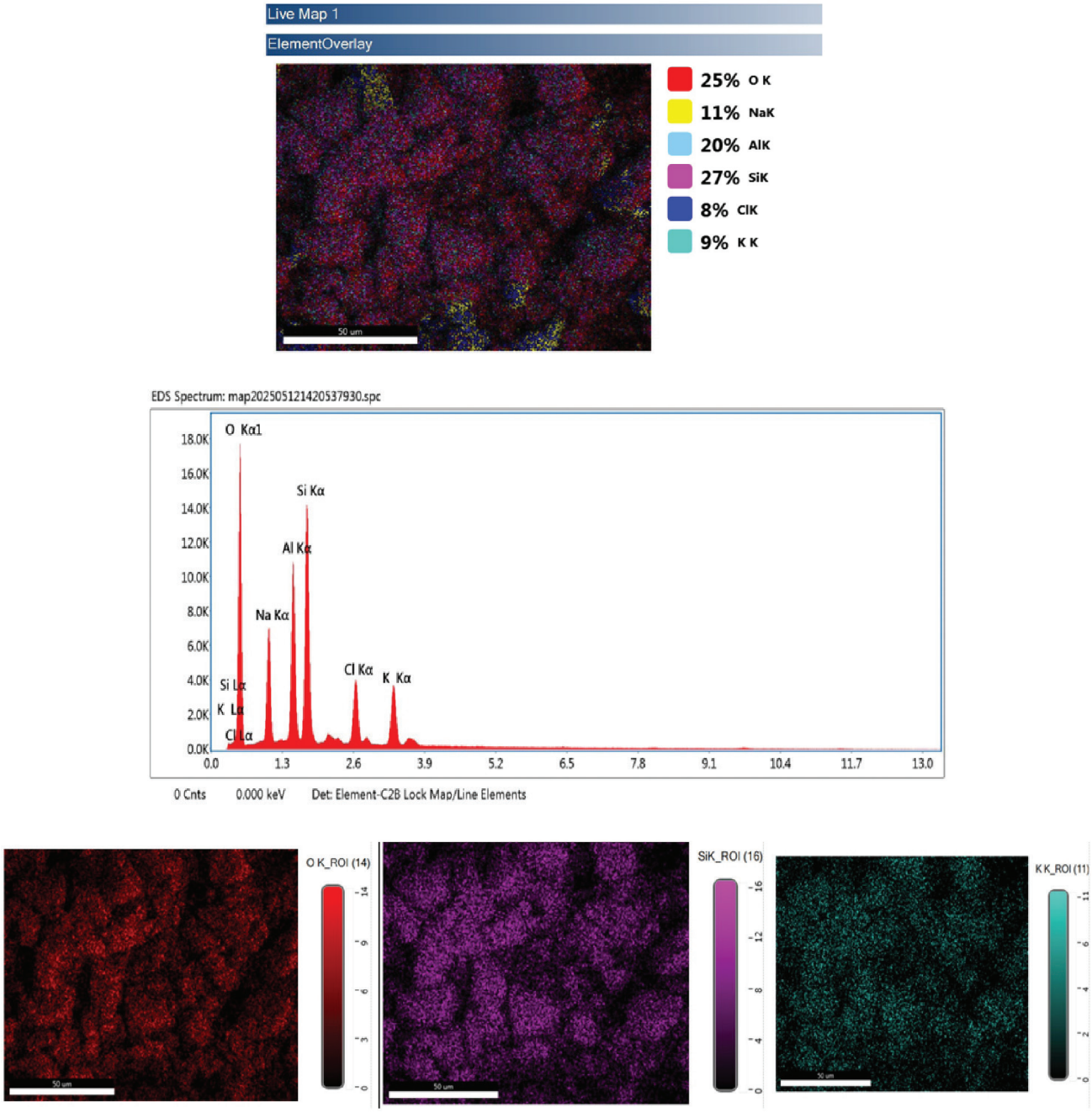

Fig. 5 – *EDS spectrum and elemental mapping of groundnut shell—derived silica nanoparticles before and after Cr(VI) adsorption*

effect of pH (Welch's ANOVA, F = 69.38, df = 6, 3.00, p = 0.0026) with achieved power of ≈ 1.00 at α = 0.05. Post-hoc comparisons to pH 4 were conducted using Welch t-tests with Holm-adjusted family-wise error control (Dunnett-style). The removal efficiency at pH 2 was significantly lower than at pH 4 (87.60 %, 95 % CI from duplicates) (Δ = −43.75 %, t = −18.90, df = 1.91, p_adj = 0.0207; Hedges' g = −10.80, 95 % CI = [−13.37, −8.22]). Differences observed at pH 3 (Δ = −9.04 %, t = −5.00, df = 1.85, p_adj = 0.1317; g = −2.86, 95 % CI = [−5.51, −0.20]), pH 5 (Δ = −2.53 %, t = −1.74, df = 1.45, p_adj = 0.5274; g = −0.64, 95 % CI = [−3.55, 2.28]), pH 6 (Δ = −4.70 %, t = −3.00, df = 1.54, p_adj = 0.3662; g = −1.43, 95 % CI = [−4.36, 1.50]), pH 7 (Δ = −6.15 %, t = −1.45, df = 1.26, p_adj = 0.3463; g = −0.83, 95% CI = [−5.35, 3.69]) and pH 8 (Δ = −18.80 %, t = −11.63, df = 1.47, p_adj = 0.1003; g = −6.64, 95 % CI = [−10.18, −3.11]) did not reach adjusted significance at α = 0.05. Complete statistical details are provided in Table 2, while the observed disparities are illustrated in Fig. 7.

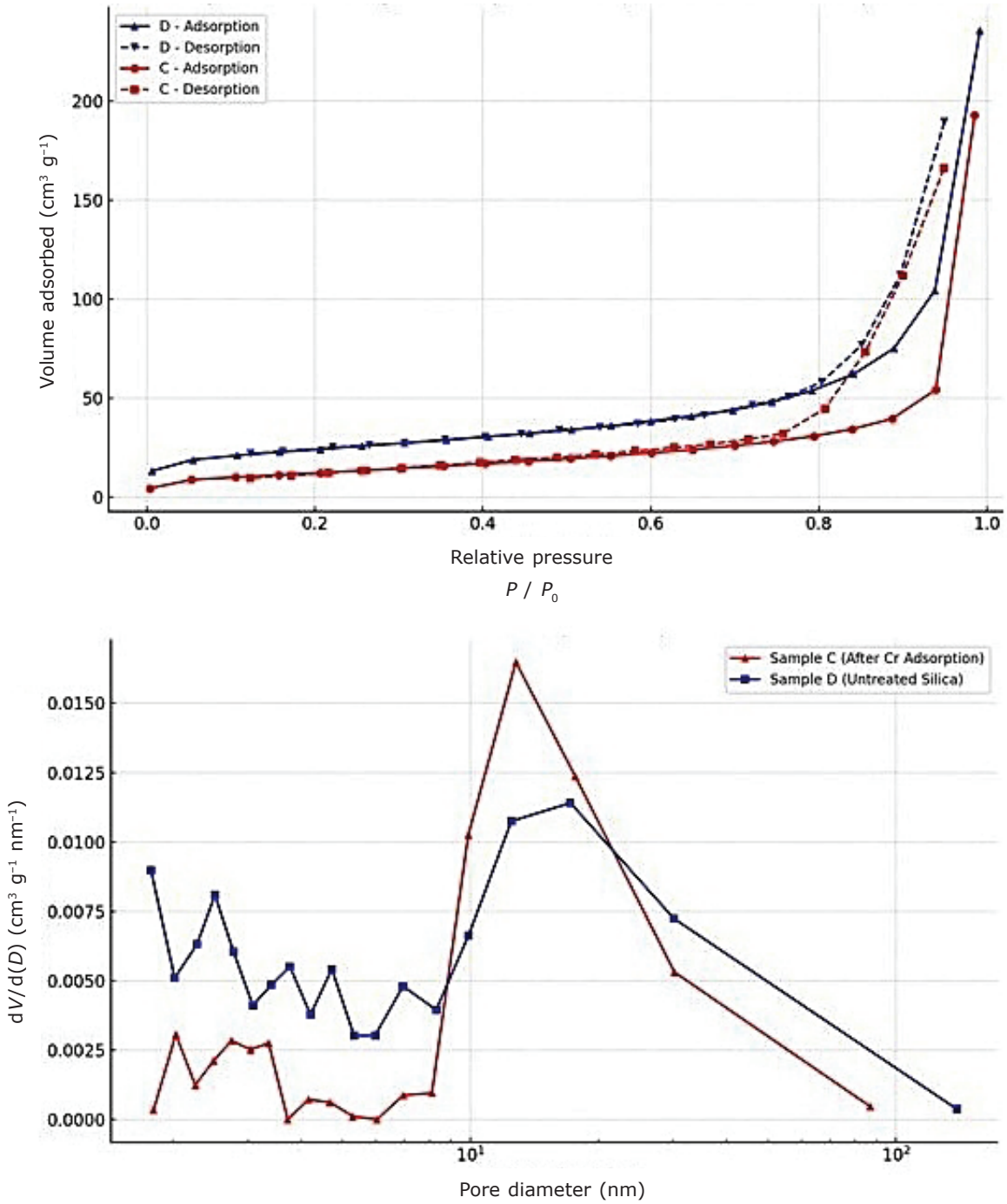

Fig. 6 – *Nitrogen adsorption—desorption isotherms and pore size distribution of groundnut shell—derived silica nanoparticles before and after Cr(VI) adsorption*

Effect of contact time

Contact time is one of the most critical factors influencing adsorption efficiency. The effect of contact duration on Cr(VI) adsorption by groundnut shell-derived silica was studied using a 10 mg L^{-1} chromium solution over a time range of 30 to 180 min. As shown in Fig. 8, chromium adsorption increased with time until equilibrium was reached at 90 minutes. The rapid initial adsorption was due to the availability of a large number of vacant sites, whereas the subsequent plateau resulted from saturation of adsorbed sites. The optimum contact time was identified as 90 minutes with adsorption efficiency of 92 %. A reduction in efficiency to 85.8 % at 180 minutes, following a minor decline after 90 minutes, maybe attributed to desorption processes or saturation of surface sites. Many bio-sorption systems exhibit a rapid initial absorption followed by a plateau, with equilibrium often being reached

Table 1 – *Functional group analysis of groundnut shell silica*

Wavenumber (cm^{-1})	Vibration type	Functional group/Assignment	Observation
3740–3360	O–H stretching (broad)	Hydroxyl groups (–OH) from cellulose, hemicellulose, and silanol groups (Si–OH)	Shift and broadening after Cr adsorption
2948–2881	C–H stretching	Aliphatic $–CH_2$ groups from organic matter	No major shift
2313–2314	–	Atmospheric CO_2 or overtone region	Unchanged
1649	H–O–H bending (δ H_2O) / C=O stretching	Adsorbed water or carbonyl groups	Slight increase after Cr adsorption
1555–1421	C=C stretching / C–O–H bending	Lignin structure and associated groups	Minor shifts
1138–1141	Si–O–Si asymmetric stretching	Silica (SiO_2) network	Present in both samples
980	Cr–O stretching / Si–OH deformation	Cr interaction or silica-related vibration	Slight shift and increase after Cr adsorption
850–725	Si–O–Si symmetric stretching / Cr–O vibration	Silica network and possible metal-oxygen bonds	More pronounced after Cr adsorption
580–440	Si–O bending	Silica structure	Present in both

Table 2 – *Robust ANOVA (Welch) and post-hoc comparisons (Dunnett-style vs control)*

Factor	Levels (control in bold)	Welch's ANOVA (F, df1, df2, p)	Achieved power	Dunnett-style post-hoc vs control (Welch t; Holm-adjusted p)	Hedges' g (95 % CI)
pH	2, 3, 4, 5, 6, 7, 8	F = 69.38, df = 6, 3.00, p = 0.0026	≈ 1.00	2 vs 4: t = −18.90, p_adj = 0.0207; 3 vs 4: t = −5.00, p_adj = 0.1317; 5 vs 4: t = −1.74, p_adj = 0.5274; 6 vs 4: t = −3.00, p_adj = 0.3662; 7 vs 4: t = −1.45, p_adj = 0.3463; 8 vs 4: t = −11.63, p_adj = 0.1003	2 vs 4: −10.80 [−13.37, −8.22] 3 vs 4: −2.86 [−5.51, −0.20] 5 vs 4: −0.64 [−3.55, 2.28] 6 vs 4: −1.43 [−4.36, 1.50] 7 vs 4: −0.83 [−5.35, 3.69] 8 vs 4: −6.64 [−10.18, −3.11]
Contact time	30, 60, 90, 120, 150, 180	n/a (single measurement per level)	n/a	n/a	n/a
Initial concentration	10, 15, 20, 25, 30, 35, 40, 45, 50, 55, 60, 65, 70	n/a (single measurement per level)	n/a	n/a	n/a
Dosage (g L^{-1})	0.2, 0.4, 0.6, 0.8, 1.0, 1.2, 1.4, 1.6, 1.8, 2.0	n/a (single measurement per level)	n/a	n/a	n/a

"n/a" = not applicable due to single observation per level

within 60–120 minutes[17,36,37]. These results confirm that 90 min is the optimal contact time for achieving maximum Cr(VI) removal using the synthesized bio-silica. Similar observations were reported by Mifti Hulijana *et al.*[37] who evaluated Cr(VI) removal using rice husk-derived silica and reported an optimum contact time consistent with this study.

The expected rise-to-plateau behavior was evident in the contact-time profiles (30–180 min), with peak removal (92.08 %) occurring at 90 min, followed by a slight decline at longer durations (120–180 min). Group-wise inferential tests (Welch's ANOVA/Dunnett) could not be performed due to the absence of replicate measurements since the optimization sheet only included one measurement at each time level (n = 1 per group). Therefore, non-parametric LOESS smoothing with bootstrap ribbons (generated by resampling residuals from the calibration curve), was employed to visualize uncertainty and provide precise point estimates without altering the experimental values. Time-wise Welch ANOVA and Dunnett comparisons are reported as not applicable (n per level = 1) in Table 2.

Effect of initial concentration

As shown in Fig. 9, increasing the initial Cr(VI) concentration resulted in a progressive decrease in removal efficiency. At a lower concentration of 10 mg L^{-1}, the removal efficiency was 92.8 %, whereas at a higher concentration of 50 mg L^{-1}, it decreased to 59 %. The adsorption capacity of the Cr(VI) ion increased as the initial concentration increased.

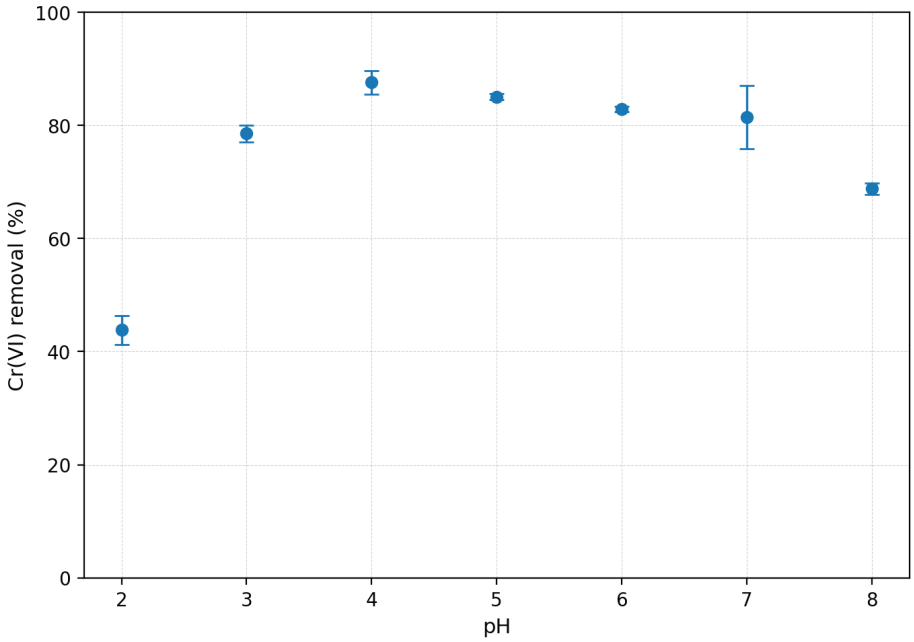

Fig. 7 – *Effect of pH on Cr(VI) removal by groundnut shell-derived silica nanoparticles*

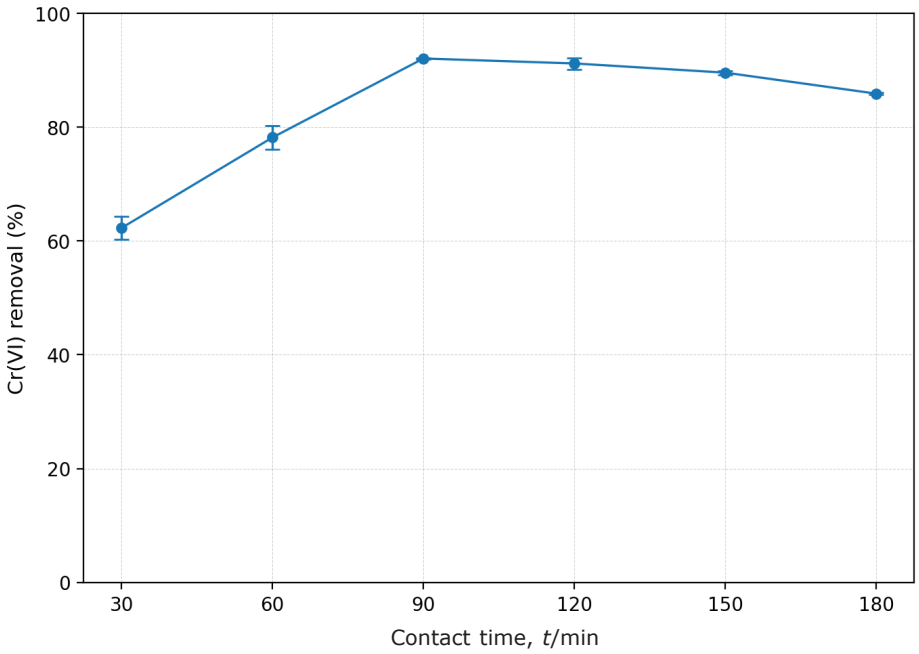

Fig. 8 – *Effect of contact time on Cr(VI) removal by groundnut shell-derived silica nanoparticles*

Subsequently, the system reached equilibrium, indicating that hexavalent chromium extraction from the solution had ceased. At higher concentrations, adsorption sites became saturated, resulting in reduced removal efficiency, whereas at lower concentrations, the available sites can interact with all metal ions, yielding greater efficiency[38,39]. In contrast, as the Cr(VI) ion concentration increased, the limited number of adsorptive sites became a limiting factor, thereby reducing the overall removal efficiency.

In the range of 10–70 mg L^{-1}, Q_e increased towards a plateau, whereas the percentage of removal declined as Ci increased, which is consistent with

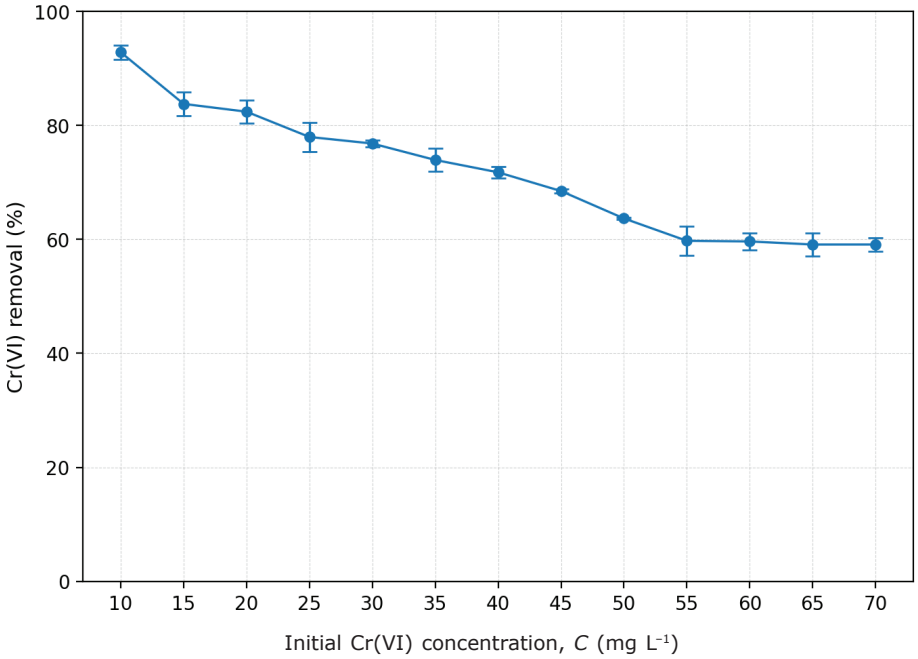

Fig. 9 – *Effect of initial Cr(VI) concentration on removal efficiency by groundnut shell-derived silica nanoparticles*

site saturation at higher loadings. Similar to contact time optimization, the concentration series included only one observation per level, making formal group-wise inference (Welch's ANOVA/Dunnett) impossible. Accordingly, without altering the current results, we saved our exact experimental values, and when new replicates were added, descriptive stream plots and/or violin-box overlays were presented to illustrate distribution shape, as shown in Fig. 9.

Effect of adsorbent dosage

Cr(VI) adsorption increased rapidly as the adsorbent dosage was raised from 0.2 to 1.0 g L^{-1}, after which it remained constant. The Cr(VI) removal efficiency increased from 39.5 % to 92 %. This improvement is attributed to the increased number of available adsorption sites and larger effective surface area at higher adsorbent dosages. However, further increases in dosage beyond 1.0 g resulted in a decline in removal efficiency. This decrease may be explained by adsorbent particle agglomeration, which reduced the effective surface area and limited accessibility to active sites. The gradient of concentration between the solute and the adsorbent surface may also diminish with increasing adsorbent dosage, thereby decreasing the driving force for mass transfer[5].

The statistical analysis of the experimental data revealed that factors such as solution pH, contact time, adsorbent dosage, and initial Cr(VI) concentration had a statistically significant effect on adsorption performance. ANOVA confirmed that the impact of pH on Cr(VI) removal efficiency was quite significant ($p < 0.05$), thus supporting the maximum removal at pH 4 that was observed experimentally. Likewise, contact time and adsorbent dosage were also found to have statistically significant effects ($p < 0.05$), hence supporting the choice of 90 min and 1 g L^{-1} as the best operating conditions. On the other hand, if the variations go beyond the optimal ranges, they will lead to a decrease in the yield because of surface saturation and particle agglomeration.

Removal efficiency increased rapidly with dosage screening (0.2–2.0 g L^{-1}) up to 1.0 g L^{-1} = 90.88 %. Agglomeration and decreased site accessibility caused a minor decline (e.g., 2.0 g L^{-1} = 85.65 %). Welch's ANOVA and Dunnett post-hoc versus 1.0 g L^{-1} could not be estimated from the current worksheet because only one observation was available at each dosage level. Therefore, a violin-box visualization with superimposed bootstrap interval estimates was used to preserve the original values, as shown in Fig. 10.

Adsorption kinetics

Kinetic studies provided insight into adsorption mechanisms, rate-controlling steps, and overall removal efficiency. The kinetic models of pseudo-first and pseudo-second order are suitable for summarizing adsorption reactions. The kinetics of adsorption

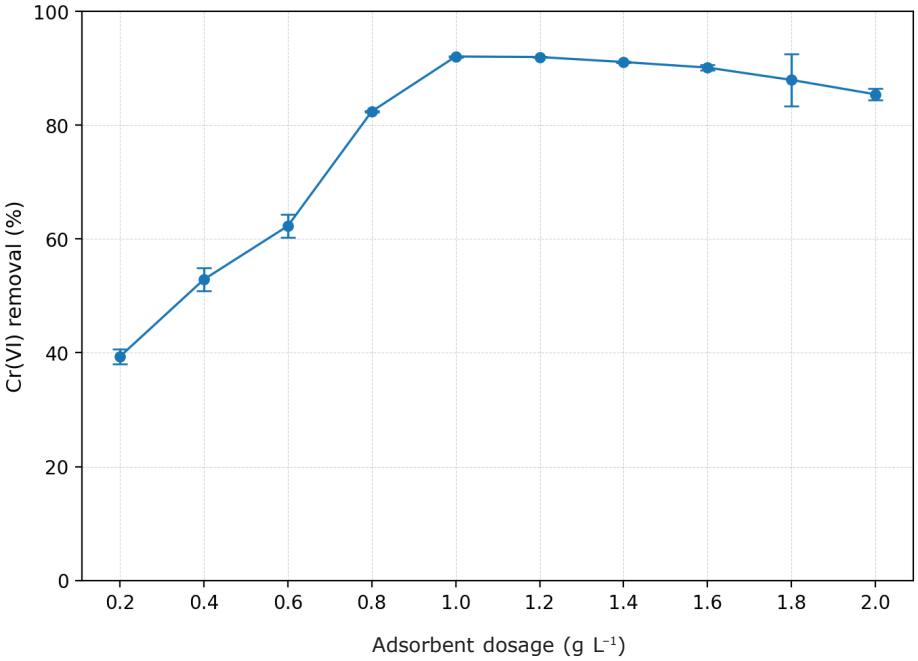

Fig. 10 – *Effect of adsorbent dosage on Cr(VI) removal efficiency by groundnut shell-derived silica nanoparticles*

are governed by a proportionate connection between the density of occupied sites and the square of the number of vacant sites[40]. In this study, chromium adsorption onto groundnut shell-derived silica was evaluated over a contact time range of 0–180 min at an initial concentration of 10 mg L^{-1}, adsorbent dosage of 1 g mL^{-1} and pH 4. The adsorption rate increased rapidly during the initial stage before reaching equilibrium at ninety minutes, after which it remained nearly constant. To assess the rate of chromium adsorption onto groundnut shell silica, pseudo-first order, pseudo-second order, and Elovich kinetic models were applied to the experimental data.

Pseudo-first order kinetics

The pseudo-first order kinetic model describes adsorption processes that are primarily governed by diffusion and rapid adsorption of the adsorbent from solution. The model is expressed by Eqn. 6, as follows:

$$\ln\left(q_e - q_t\right) = \ln q_e - K\,t \tag{6}$$

where K_1 is the pseudo-first order rate constant, q_t (mg g^{-1}) is the amount of Cr(VI) in a given time, and q_e (mg g^{-1}) is the equilibrium amount of Cr(VI) adsorption.

The K_1 values for different concentrations range from 0.0853, while the R^2 values range from 0.0324, which indicates very low R^2 values in comparison to other kinetics. Deviation from linearity in the adsorption kinetics data suggests that the chromium adsorption onto the silica is not well described by the pseudo-first-order kinetics. Similar results were reported when silica was used to adsorb chromium from volcanic ash[41].

Pseudo-second order kinetics

As the rate-limiting stage in the adsorption process, the pseudo-second order model explains how chemical adsorption affects electrostatic forces. Eqn. 7 indicates the equations that were used to calculate the pseudo-second-order kinetics.

$$\frac{1}{q_t} = \frac{1}{K_2 q_e^{\,2}} + t\frac{1}{q_e} \tag{7}$$

Eqn. (7) adheres to pseudo-second-order kinetics when K_2 is used as the rate constant. (t/q_t) was used to plot Fig. 11 versus t. A better fit is indicated by higher R^2 value ($R^2 \approx 0.99$), and the rate of adsorption in Table 3, which represents pseudo-second-order kinetics, was modified by chemisorption. The results presented here are supported by a chemisorption process that is compatible with the kinetic adsorption behavior detailed in references[29,41].

Elovich kinetics

According to the Elovich model, the surface is heterogeneous and second-order kinetics are supported. The following equation was used to calculate the Elovich kinetics analysis. Eqn. (8) was used to obtain the adsorption capacity, where β stands for

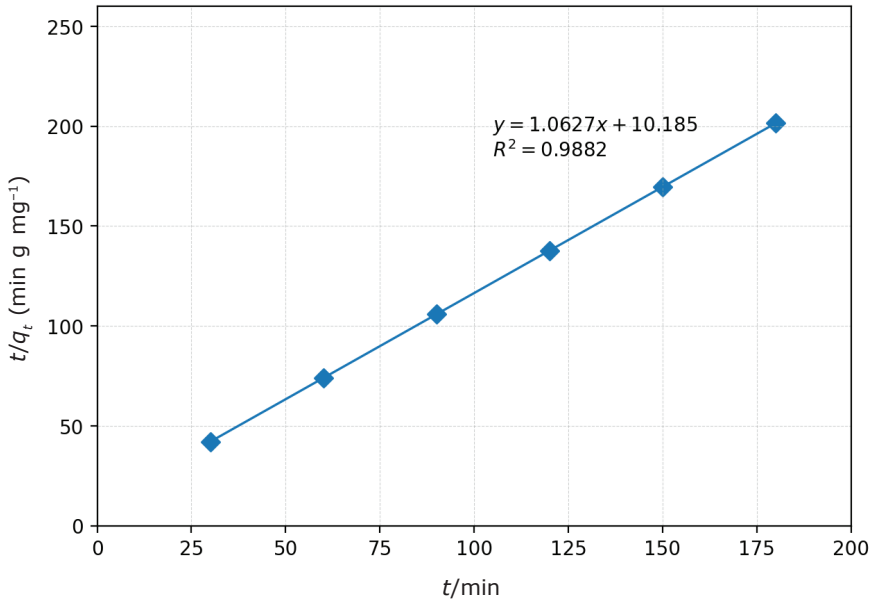

Fig. 11 – *Pseudo-second-order kinetic plot for Cr(VI) adsorption onto groundnut shell-derived silica nanoparticles*

Table 3 – *Adsorption kinetics*

Model	Rate constant/Slope	Intercept	R^2	Interpretation
Pseudo-first-order	K_1 = 0.00853 min^{-1}	–2.947	0.0324	Poor fit, not applicable
Pseudo-second-order	$1/q_e$ = 1.063	10.19	0.9882	Best fit, indicates chemisorption
Elovich	$1/\beta$ = 0.1439 A = 0.627 mg g^{-1} min^{-1}	0.186	0.8871	Moderate fit, supports surface interaction

the desorption constant, and α for the initial adsorption rate.

$$q_t = \frac{1}{\beta}\ln(\alpha\beta) + \frac{1}{\beta}\ln t \quad (8)$$

Therefore, assuming adsorption data fit the model, a plot of q_t against ln(t) would provide a straight line. The plots' intercept and slope, respectively, can be used to calculate the variables α and β. The Elovich kinetic plot is given in Fig. 12.

A straight line with a slope of $1/\beta$=0.1439 and an intercept of 0.186 was produced by plotting q_t against ln t. The Elovich constants, which stand for the desorption rate constant and the initial adsorption rate, respectively, were determined using these values as β=6.95 g mg^{-1} and α=0.627 mg g^{-1} min^{-1}. The regression coefficient R^2=0.8871 shows a moderately satisfactory fit, suggesting that the Elovich model suitably describes the Cr(VI) adsorption process onto silica. The results suggest that adsorption occurs on a heterogeneous surface and is influenced by chemisorption involving surface interactions[42].

The pseudo-second-order model best describes the kinetic data for Cr(VI) adsorption onto silica, suggesting a mechanism driven by chemisorption. While the Elovich model's reasonably good fit further highlights the significance of surface interactions on a heterogeneous adsorbent, the pseudo-first-order model was found to be unsuitable for defining the system.

Adsorption isotherm investigation

Langmuir isotherm

The Langmuir isotherm describes monolayer sorption onto the surface of an adsorbent with a small number of identical adsorption sites and no interactions between them[43]. To evaluate the model's ability to replicate the interactions between the adsorbent and the bio-sorbent surface, the adsorption of chromium ions onto groundnut silica was investigated using the Langmuir isotherm. The linear and nonlinear forms of the Langmuir equation are represented by Eqs. 9 (a and b).

$$\frac{C_e}{q_e} = \frac{1}{q_m} C_e + \frac{1}{K_L q_m} \tag{9a}$$

$$q_e = \frac{q_m K_L C_e}{1 + K_L C_e} \tag{9b}$$

where q_m is the maximum adsorption capacity (mg g^{-1}), and K_L is the Langmuir constant (L mg^{-1}). The plot of C_e/q_e versus C_e in (Fig. 13) exhibited a linear pattern with a strong correlation coefficient (R^2=0.9693) suggesting that the Langmuir model provided a fair preliminary account of the adsorption kinetics. The maximum adsorption capacity (q_m) of 4.5955 mg g^{-1} and the Langmuir constant (K_L) of 0.1568 L mg^{-1} (calculated from the slope and intercept, respectively) suggest a moderate affinity between the chromium ions and the groundnut silica[44]. On the other hand, nonlinear regression of the original Langmuir equation was applied to evaluate the Langmuir model further, as linearizа-

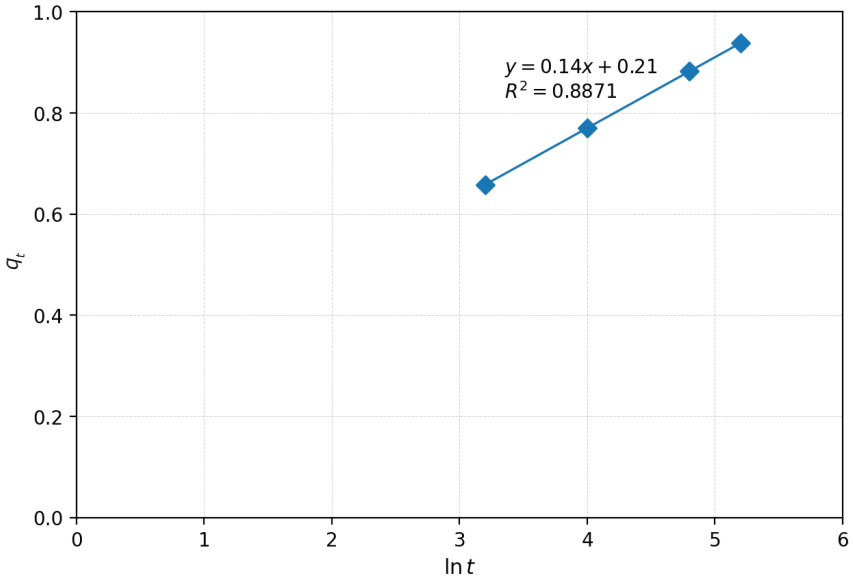

Fig. 12 – *Elovich kinetic plot for Cr(VI) adsorption onto groundnut shell-derived silica nanoparticles*

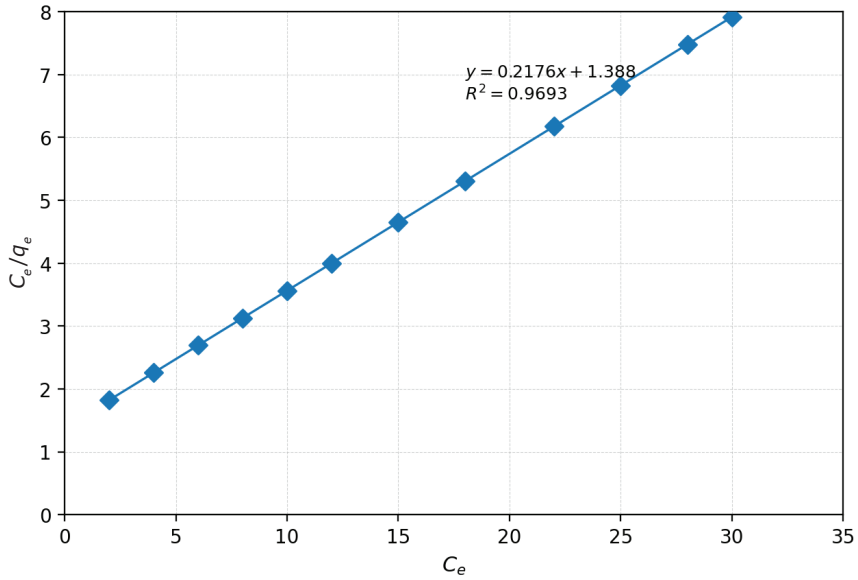

Fig. 13 – *Langmuir isotherm plot for Cr(VI) adsorption onto groundnut shell-derived silica nanoparticles*

tion could generate statistical bias. The nonlinear fit yielded an RMSE of 0.210 mg g^{-1} and a chi-square (χ^2) value of 0.574, thus, reporting significant discrepancies between the experimental and predicted adsorption capacities. These findings suggest that the Langmuir model can still characterize the adsorption equilibrium to a certain degree[44], but does not deliver the most accurate representation of the experimental data; hence, it can be concluded that adsorption is not always confined to the ideal monolayer coverage situation.

Freundlich isotherm

The Freundlich isotherm is the first known relationship that describes reversible and non-ideal adsorption that is not limited to monolayer formation. With a heterogeneous surface and an uneven distribution of adsorption heat and affinities, this empirical model can be used for multilayer adsorption[45]. This research investigated the adsorption of chromium ions onto groundnut silica, using the Freundlich model of adsorption. The linear and nonlinear forms of the Freundlich equation are represented by Eqs. 10 (a and b).

$$\log q_e = \frac{1}{n}\log C_e + \log K_F \qquad (10a)$$

$$q_e = K_F C_e^{\,1/n} \qquad (10b)$$

where K_F is the Freundlich constant (mg g^{-1}), and n is the adsorption intensity. The log q_e versus log C_e plot, as depicted in Fig. 14, yielded a linear regression line with a high R^2 value of 0.9826, suggesting that the Freundlich model fitted the data well. The values of n and K_F were calculated from the plot's slope and intercept, respectively; n = 2.4396 and K_F = 0.9975. To obtain a more reliable assessment, nonlinear regression of the original Freundlich equation was performed using the q_e and C_e experimental data. The nonlinear fitting yielded the lowest RMSE (0.134 mg g^{-1}) and χ^2 (0.089) values among all tested models. The close agreement between experimental and predicted values across the entire concentration range confirms that the Freundlich model provided the most accurate description of Cr(VI) adsorption onto groundnut shell–derived silica. This behavior reflects surface heterogeneity and non-uniform energy distribution of adsorption sites, which is characteristic of bio-silica based adsorbents. Adsorption is most favorable when $n > 1$. The adsorption behavior observed in this study indicated that groundnut shell-derived silica possesses a heterogeneous surface capable of multilayer adsorption. Based on the strong correlation and favorable adsorption values, the Freundlich model provides an appropriate description of the chromium adsorption equilibrium in this study[44].

Temkin isotherm

The Temkin isotherm considers how the interactions between adsorbates change the process of adsorption. It assumes that the adsorbent and adsorbate interact, that the heat of adsorption decreases linearly with surface coverage, and that the binding energy is evenly distributed across the adsorbent surface[46]. For this study, we used the linear and

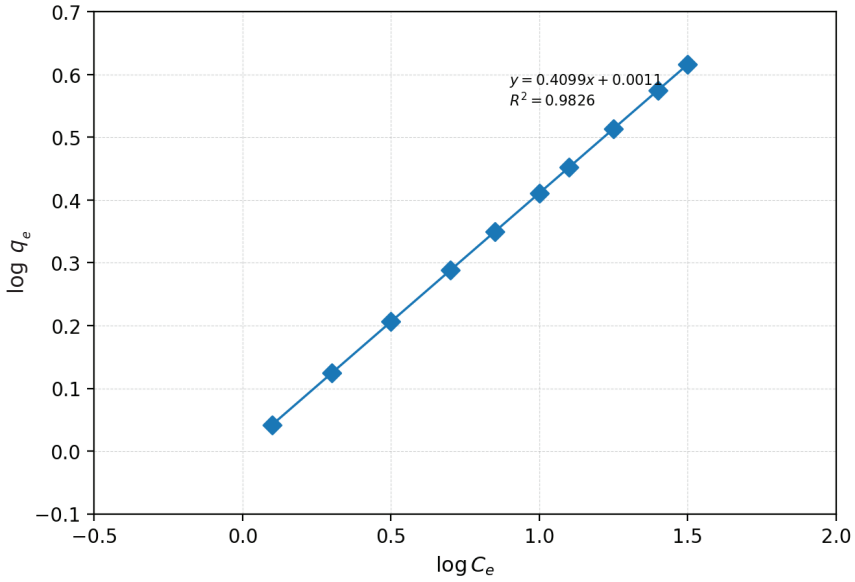

Fig. 14 – *Freundlich isotherm plot for Cr(VI) adsorption onto groundnut shell-derived silica nanoparticles*

nonlinear forms of the Temkin equation to explain how chromium ions adhere to groundnut silica:

$$q_e = \frac{RT}{b_T}\ln C_e + \frac{RT}{b_T}\ln K_T \quad (11a)$$

$$q_e = \frac{RT}{b_T}\ln K_T C_e \quad (11b)$$

The Temkin constant for the heat of adsorption (J mol^{-1}) is b_T, the Temkin isotherm constant (L g^{-1}) is K_T, the universal gas constant (8.314 J mol^{-1} K^{-1}) is R, and the absolute temperature (K) is T. Fig. 15 shows that q_e and ln C_e are linearly related, with a coefficient of determination of R^2=0.9375. The slope and intercept of the plot revealed a heat of adsorption (b_T) of 2854.99 J mol^{-1}. The Temkin constant (K_T), according to the equilibrium binding energy, was derived as 2.2766 L g^{-1}. Nonlinear fitting of the original Temkin equation resulted in a comparatively higher RMSE of 0.244 mg g^{-1} and χ^2 of 0.776, indicating poorer agreement with the experimental data. The larger deviations, particularly at low and high equilibrium concentrations, suggest that the Temkin model is less suitable for describing Cr(VI) adsorption on the present bio-silica material. This suggests a moderate interaction between the chromium ions and the surface of the groundnut shell-derived silica. Although the Temkin model had a lower R^2, and higher RMSE and χ^2 values than the Freundlich model, the Temkin model provides a valuable thermodynamic explanation of the adsorption behavior in this system.

Chemically functionalized and composite silica-based materials have been widely investigated for Cr(VI) removal, where adsorption is governed by surface interactions between chromium oxyanions and active functional groups on the silica framework[47]. Surface functionalization of mesoporous silica has been reported to significantly enhance Cr(VI) adsorption, particularly under acidic conditions due to favorable electrostatic interactions[47]. Iron oxide–silica nanocomposites with high surface area have also demonstrated effective Cr(VI) removal, with adsorption behavior well described by Langmuir and Freundlich isotherms and pseudo-first- and pseudo-second-order kinetic models, indicating surface-controlled adsorption mechanisms[48]. Additionally, functional porous silica nanoparticles have been shown to retain adsorption efficiency over multiple reuse cycles, highlighting their practical applicability in water treatment systems[49].

Rice husk–derived silica adsorbents reported in the literature typically exhibit moderate to high Cr(VI) removal efficiencies under strongly acidic conditions (pH ≈ 2–3) and often require higher adsorbent dosages or specific operating parameters[50–52]. In comparison, the groundnut shell–derived silica developed in the present study achieved high Cr(VI) removal efficiency at comparable initial concentrations under mildly acidic conditions (pH 4) without chemical functionalization. This combination of efficient removal, reduced acidity requirement, and simpler material preparation highlights the improved practical applicability of groundnut shell silica for chromium remediation. Comparative statistical analysis confirmed the pseudo-second-order kinetic model and the Freundlich isotherm as

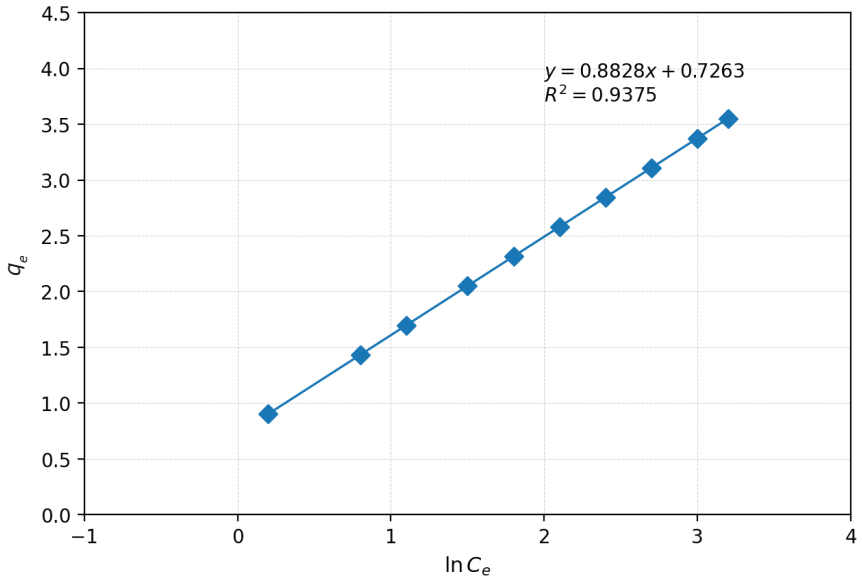

Fig. 15 – *Temkin isotherm plot for Cr(VI) adsorption onto groundnut shell-derived silica nanoparticles*

Table 4 – *Isotherm models and factors*

Isotherm model	Linear parameters	R^2 (linear)	Nonlinear parameters	RMSE (mg g^{-1})	χ^2
Langmuir	q_m = 4.5955 mg g^{-1} K_L = 0.1568 L mg^{-1}	0.9693	q_m = 4.68 mg g^{-1} K_L = 0.142 L mg^{-1}	0.210	0.574
Freundlich	K_F = 0.9975 n = 2.4396	0.9826	K_F = 1.004 n = 2.45	0.134	0.089
Temkin	b_T = 2854.99 J mol^{-1} K_T = 2.2766 L g^{-1}	0.9375	b_T = 2854.99 J mol^{-1} K_T = 2.2766 L g^{-1}	0.244	0.776

the best and most appropriate representations of the experimental data. Their superiority was evidenced by the highest correlations and minimal error values among the models tested. The model differences in performance were consistent throughout the fit quality indicators, such asreduced residual dispersion and improved predictive accuracy. These findings further confirm the validity of the chosen kinetic and isotherm models for the description of Cr(VI) adsorption onto groundnut shell-derived silica. Comprehensive statistical metrics, including Akaike Information Criterion (AIC), Root Mean Square Error (RMSE), and residual analyses, are provided in the Supplementary Material.

Adsorption mechanism

The interaction between Cr(VI) and groundnut shell-derived silica is strongly supported by structural and surface analyses. FTIR spectra revealed shifts in the O–H stretching region (~3400 cm^{-1}) and the emergence of a peak at 980 cm^{-1} after adsorption, indicating that Cr(VI) ions chemically interacted with surface hydroxyl and silanol groups, likely through complexation or hydrogen bonding. SEM images showed a morphological transformation from a rough, porous surface to a smoother, less porous structure post-adsorption, while BET analysis confirmed a notable reduction in pore volume diameter and surface area, suggesting pore diffusion and surface occupation by Cr(VI) ions. Additionally, XRD patterns indicated increased crystallinity, and EDS analysis verified the presence and even distribution of chromium, confirming its effective immobilization on the silica surface.

The process exhibited pseudo-second-order kinetics (R^2 = 0.99), according to kinetic modeling, indicating that chemisorption through electron sharing or exchange was the rate-limiting phase. The ideal fit among the isotherm models was given by the Freundlich model (R^2 = 0.9826), which suggested heterogeneous and multilayer adsorption. An excellent fit was also demonstrated by the Langmuir model (R^2 = 0.9693), suggesting partial monolayer adsorption on homogeneous high-energy active sites. By taking into consideration adsorbate–adsorbent interactions, the Temkin isotherm (R^2 = 0.9375) provided additional evidence for the process, as shown in Table 4. Its linear decline in adsorption heat indicated a moderate binding energy between the silica surface and Cr(VI) ions.

Additionally, the adsorption efficiency was strongly pH-dependent, with pH 4 yielding the highest Cr(VI) removal. At this pH, electrostatic attraction is promoted because the bio-silica surface is protonated and Cr(VI) is mostly present as $HCrO_4^-$. At lower pH levels, competition from H^+ ions reduced adsorption efficiency, whereas at higher pH values, surface deprotonation reduced affinity for anionic Cr(VI) species. The overall adsorption of Cr(VI) onto groundnut shell-derived silica was governed by a chemisorption-driven mechanism involving surface complexity, electrostatic attraction, pore diffusion, and heterogeneous multilayer interactions, all supported by a mesoporous, functionally rich bio-silica matrix. The pseudo-second-order kinetic fitting (R^2 = 0.99) and Freundlich isotherm conformity (R^2 = 0.9826) that favored the Cr(VI) adsorption on groundnut shell-derived silica with pseudo-second-order kinetics and adsorption through chemisorption and heterogeneity, suggest the possibility of an adsorption process dominated by chemisorption and heterogeneous adsorption. Nevertheless, advanced surface-sensitive techniques such as X-ray photoelectron spectroscopy (XPS) and zeta potential analysis could provide more definitive evidence of surface complexation and electrostatic interactions. The absence of these analyses represents a limitation of this study. However, the combined results from kinetic, isotherm, and FTIR analyses are internally consistent and can be considered reliable for interpreting the adsorption mechanism.

Conclusion

This study demonstrates the effective removal of hexavalent chromium from aqueous solutions using bio-silica derived from groundnut shells as an inexpensive and sustainable adsorbent. Structural analysis using FTIR and XRD confirmed the pres-

ence of silica and indicated that chromium was successfully adsorbed through interactions with surface hydroxyl groups. EDS and elemental mapping confirmed the homogeneous distribution of key elements, whereas SEM analysis revealed significant morphological changes after adsorption, including surface smoothing and reduced porosity. By verifying pore blockage and interaction after chromium uptake, BET analysis provided additional support for the adsorption process by demonstrating notice able reductions in pore volume, pore diameter, and surface area.

The removal of Cr(VI) was shown to be highly dependent on contact time, pH, initial concentration, and adsorbent dosage, with the best removal occurring at pH 4 and 90 minutes, according to adsorption experiments. Although slight decreases were observed at very high dosages due to particle agglomeration, the system exhibited optimal removal efficiency at lower chromium concentrations and higher adsorbent dosages. Kinetic modeling revealed that adsorption followed pseudo-second-order kinetics (R^2 = 0.99), indicating that chemisorption governed the rate-limiting phase. Although the Langmuir and Temkin models also showed a significant adsorption capacity and moderate interaction energies, the Freundlich isotherm offered the best fit among the isotherm models used (R^2 = 0.9826) with the lowest χ^2 (0.089) and RMSE value (0.134), suggesting multilayer adsorption on a heterogeneous surface. Overall, groundnut shell-derived silica showed considerable promise as an effective and sustainable adsorbent for Cr(VI) removal, driven by a chemisorption-based mechanism on a mesoporous and functionally active surface. Future research will primarily focus on adsorbent regeneration and reusability using suitable desorbing agents, evaluation of performance with real industrial effluents, and cost-benefit analysis to determine material stability, scalability, and industrial applicability.

Supplementary

Model selection and error analysis

To strengthen the kinetic and equilibrium models used in this study, additional statistical performance indicators were employed, including the Akaike Information Criterion (AIC), root mean square error (RMSE), and residual error analysis. These metrics evaluate model suitability in terms of goodness-of-fit, predictive accuracy, and model parsimony, providing complementary insight alongside correlation coefficients.

S1. Akaike Information Criterion (AIC)

The Akaike Information Criterion (AIC) was used to compare competing kinetic and isotherm models where model complexity is weighed against goodness-of-fit. Lower AIC values indicate superior model performance with minimal information loss. Among the kinetic models evaluated, the pseudo-second-order kinetic model showed the lowest AIC value, confirming its statistical superiority over the pseudo-first-order and Elovich models. Similarly, the Freundlich isotherm model produced the minimum AIC value compared with the Langmuir and Temkin models, confirming its suitability for describing Cr(VI) adsorption onto groundnut shell-derived silica.

S2. Root Mean Square Error (RMSE)

RMSE was used to quantify the extent of the difference between adsorption values proposed by the model and those obtained experimentally. A lower RMSE indicates higher predictive accuracy. The pseudo-second-order kinetic model exhibited the lowest RMSE value, demonstrating the closest agreement between experimentally measured adsorption capacities and model predictions over the entire contact time range. In equilibrium modeling, the Freundlich isotherm also yielded the lowest RMSE, further supporting its applicability to heterogeneous multilayer adsorption.

S3. Residual Error Analysis

Residual analysis involved examining the distribution of residuals (i.e., difference between experimental and predicted values) for all evaluated models. The pseudo-second-order kinetic and Freundlich isotherm models displayed randomly distributed residuals without systematic trends, indicating the lack of model bias and the suitability of these models. In contrast, the residuals associated with other models were larger, especially at higher adsorption capacities, indicating reduced prediction reliability.

S4. Statistical Consistency with Main Text Findings

The combined evaluation of AIC, RMSE, and residual distributions consistently reinforces the main findings of this study: Cr(VI) adsorption onto groundnut shell–derived silica is best described by the pseudo-second-order kinetic model and the Freundlich isotherm.

References

1. *Al-Huqail*, *A. A*., *Kumar*, *P., Eid*, *E. M., Adelodun*, *B., Abou Fayssal*, *S., Singh, J., Širić*, *I.,* Risk assessment of heavy metals contamination in soil and two rice (*Oryza sativa* L.) varieties irrigated with paper mill effluent, Agric. **12** (2022) 1864. doi: https://doi.org/10.3390/agriculture12111864
2. *Tchounwou*, *P. B., Yedjou*, *C. G., Patlolla*, *A. K., Sutton*, *D. J.,* Heavy metal toxicity and the environment, Mol. Clin. Environ. Toxicol. **3** (2012) 133. doi: https://doi.org/10.1007/978-3-7643-8340-4_6
3. *McCartor*, *A., Becker*, *D., Hanrahan*, *D., Ericson*, *B., Thomen*, *A., Fuller*, *R., Caravanos*, *J.,* Worlds Worst Pollution Problems Report 2010, Blacksmith Inst. **1** (2010) 1.
4. *Lewicki*, *S., Zdanowski*, *R., Krzyzowska*, *M., Lewicka*, *A., Debski*, *B., Niemcewicz, M., Goniewicz*, *M.,* The role of chromium III in the organism and its possible use in diabetes and obesity treatment, Ann. Agric. Environ. Med. **21** (2014) 2. doi: https://doi.org/10.5604/1232-1966.1108599
5. *Gupta*, *V. K., Nayak*, *A., Agarwal*, *S.,* Bioadsorbents for remediation of heavy metals: Current status and their future prospects, Environ. Eng. Res. **20** (2015) 1. https://doi.org/10.4491/eer.2015.018
6. *Tumolo*, *M., Ancona*, *V., De Paola*, *D., Losacco*, *D., Campanale*, *C., Massarelli*, *C., Uricchio*, *V. F.,* Chromium pollution in European water, sources, health risk, and remediation strategies: An overview, Int. J. Environ. Res. Public Health. **17** (2020) 5438. doi: https://doi.org/10.3390/ijerph17155438
7. *Stambulska*, *U. Y*., *Bayliak*, *M. M*., *Lushchak*, *V. I.,* Cr(VI) toxicity in legume plants: Modulation effects of rhizobial symbiosis, Biomed. Res. Int. **1** (2018) 8031213. doi: https://doi.org/10.1155/2018/8031213
8. *Thavasilingam, K., Senthil Kumar, A., Adam Khan, M., Devanand, S., Giridharan, K.,* Effect of fumed silica in rice bran wax–epoxy coating on aluminum substrate: Mechanical, thermal, and water absorption properties, Biomass Conv. Bioref. **13** (2021) 4229. doi: https://doi.org/10.1007/s13399-021-01889-w
9. *Sewalem*, *T.,* Physicochemical parameters and selected heavy metal contents of waste water effluents from soft drink factory, Burie, Gojam, Ethiopia, Ambo Univ. Diss. **1** (2022) 1.
10. *Qasem*, *N. A., Mohammed*, *R. H., Lawal*, *D. U.,* Removal of heavy metal ions from wastewater: A comprehensive and critical review, NPJ Clean Water **4** (2021) 36. doi: https://doi.org/10.1038/s41545-021-00127-0
11. *Dong*, *J., Du*, *Y., Duyu*, *R., Shang*, *Y., Zhang*, *S., Han*, *R.,* Adsorption of copper ion from solution by polyethylenimine modified wheat straw, Bioresour. Technol. Rep. **6** (2019) 96. doi: https://doi.org/10.1016/j.biteb.2019.02.011
12. *Zhao, L., Zhang, Q., Li*, *X., Ye*, *J., Chen*, *J.,* Adsorption of Cu(II) by phosphogypsum modified with sodium dodecyl benzene sulfonate, J. Hazard. Mater. **387** (2020) 121808. doi: https://doi.org/10.1016/j.jhazmat.2019.121808
13. *Kumari*, *D., Goswami*, *R., Kumar*, *M., Kataki, R., Shim*, *J.,* Removal of Cr(VI) ions from aqueous solution through nanoscale zero-valent iron (nZVI) Magnetite Corn Cob Silica (MCCS): A bio-waste based water purification perspective, Groundw. Sustain. Dev. **7** (2018) 470. doi: https://doi.org/10.1016/j.gsd.2017.12.007
14. *Edokpayi*, *J. N., Odiyo*, *J. O., Msagati*, *T. A., Popoola*, *E. O.,* A novel approach for the removal of lead (II) ion from wastewater using mucilaginous leaves of *Diceriocaryum eriocarpum* plant, Sustainability **7** (2015) 14026. doi: https://doi.org/10.3390/su71014026
15. *Ahmed*, *R., Block*, *I.,Otte*, *F., Günter*, *C., Duarte-Rodrigues*, *A., Hesemann*, *P., Taubert*, *A.,* Activated carbon from sugarcane bagasse: A low-cost approach towards Cr(VI) removal from wastewater, Chemistry **5** (2023) 1124. doi: https://doi.org/10.3390/chemistry5020077
16. *Nguyen*, *D. K., Ly-Tran*, *Q. B., Dinh*, *V. P., Duong*, *B. N., Nguyen*, *T. P. T., Tuyen*, *P. N. K.,* Adsorption mechanism of aqueous Cr(VI) by Vietnamese corncob biochar: A spectroscopic study, RSC Adv. **14** (2024) 39205. doi: https://doi.org/10.1039/D4RA07455F
17. *Bayuo*, *J., Pelig-Ba*, *K. B., Abukari, M. A.,* Adsorptive removal of Cr(VI) from aqueous solution unto groundnut shell, Appl. Water Sci. **9** (2019) 107. doi: https://doi.org/10.1007/s13201-019-0987-8
18. *Thavasilingam, K., Senthil Kumar, A., Sakthimurugan, D., Meenatchisundaram, P.,* Synthesis and characterization of fumed silica dispersed beeswax/carnauba wax–epoxy biocomposite coating: A comparative study, Biomass Conv. Bioref. **13** (2023) 7375. doi: https://doi.org/10.1007/s13399-023-04112-0
19. *Da'na*, *E.,* Adsorption of heavy metals on functionalized-mesoporous silica: A review, Microporous Mesoporous Mater. **247** (2017) 145. doi: https://doi.org/10.1016/j.micromeso.2017.03.050
20. *Akhayere*, *E., Kavaz*, *D., Vaseashta*, *A.,* Efficacy studies of silica nanoparticles synthesized using agricultural waste for mitigating waterborne contaminants, Appl. Sci. **12** (2022) 9279. doi: https://doi.org/10.3390/app12189279
21. *Meky*, *N., Salama*, *E., Soliman*, *M. F., Naeem, S. G., Ossman*, *M., Elsayed, M.,* Synthesis of nano-silica oxide for heavy metal decontamination from aqueous solutions, Water Air Soil Pollut. **235** (2024) 154. doi: https://doi.org/10.1007/s11270-024-06944-6
22. *Morales-Paredes*, *C. A., Rodríguez-Linzán*, *I., Saquete*, *M. D., Luque*, *R., Osman*, *S. M., Boluda-Botella*, *N., Manuel*, *R. D. J.,* Silica-derived materials from agro-industrial waste biomass: Characterization and comparative studies, Environ. Res. **231** (2023) 116002. doi: https://doi.org/10.1016/j.envres.2023.116002
23. *Sachan*, *D., Ramesh*, *A*., *Das*, *G.,* Green synthesis of silica nanoparticles from leaf biomass and its application to remove heavy metals from synthetic wastewater: A comparative analysis, Environ. Nanotechnol. Monit. Manag. **16** (2021) 100467. doi: https://doi.org/10.1016/j.enmm.2021.100467
24. *Jang, E. H., Pack, S. P., Kim, I., Chung, S.,* A systematic study of hexavalent chromium adsorption and removal from aqueous environments using chemically functionalized amorphous and mesoporous silica nanoparticles, Sci. Rep. **10** (2020) 5558. doi: https://doi.org/10.1038/s41598-020-61505-1
25. *Kannan, S., Thavasilingam, K., Muruga Boopathi, M., Marimuthu, K.,* Sustainable extraction and ML-based yield prediction of silica nanoparticles from sugarcane bagasse and groundnut shell for functional surface coatings, Silicon. **12** (2025) 1166. doi: https://doi.org/10.1007/s12633-025-03517-y
26. *Zhao*, *L., Zhang, Q., Li*, *X., Ye*, *J., Chen*, *J.,* Adsorption of Cu(II) by phosphogypsum modified with sodium dodecyl benzene sulfonate, J. Hazard. Mater. **387** (2020) 121808. doi: https://doi.org/10.1016/j.jhazmat.2019.121808

27. *September*, *L. A., Kheswa*, *N., Seroka*, *N. S., Khotseng, L.,* Green synthesis of silica and silicon from agricultural residue sugarcane bagasse ash–a mini review, RSC Adv. **13** (2023) 1370. doi: https://doi.org/10.1039/D2RA07490G
28. *Guevara-Lora*, *I., Wronski*, *N., Bialas*, *A., Osip*, *H., Czosnek*, *C.,* Efficient adsorption of chromium ions from aqueous solutions by plant-derived silica, Molecules **27** (2022) 4171. doi: https://doi.org/10.3390/molecules27134171
29. *Al-Qadri*, *F. A., Alsaiari*, *R., Mohamed*, *M. M., Mohamed, E., Alkorbi*, *F., Alsaiari*, *N., Rizk*, *M. A.,* Bio-sorbent of silica ash from palm frond for elimination of Cr(VI) from water sources, Indian J. Sci. Technol. **17** (2024) 979. doi: https://doi.org/10.17485/IJST/v17i11.3275
30. *Dorairaj*, *D., Govender*, *N., Zakaria*, *S., Wickneswari*, *R.,* Green synthesis and characterization of UKMRC-8 rice husk-derived mesoporous silica nanoparticle for agricultural application, Sci. Rep. **12** (2022) 20162. doi: https://doi.org/10.1038/s41598-022-24484-z
31. *Mehmood, S., Mahmood*, *M., Núñez-Delgado*, *A., Alatalo*, *J. M., Elrys*, *A. S., Rizwan*, *M., Ahmed*, *W.,* A green method for removing Cr(VI) from aqueous systems using novel silicon nanoparticles: Adsorption and interaction mechanisms, Environ. Res. **213** (2022) 113614. doi: https://doi.org/10.1016/j.envres.2022.113614
32. *Kouadri*, *I., Seghir*, *B. B., Hemmami*, *H., Zeghoud*, *S., Allag*, *N., Rebiai*, *A., Belkhalfa*, *H.,* Extraction of silica from different sources of agricultural waste, J. Pure Appl. Ind. Phys. **1** (2023) 16. doi: https://doi.org/10.52711/0974-4150.2023.00016
33. *Storck*, *S., Bretinger*, *H., Maier*, *W. F.,* Characterization of micro-and mesoporous solids by physisorption methods and pore-size analysis, Appl. Catal. A Gen. **174** (1998) 137. doi: https://doi.org/10.1016/S0926-860X(98)00164-1
34. *Thavasilingam, K., Sakthimurugan, D., Ashok, K. G., Devanand, S.,* Green synthesis of Brassica leaf extract biocomposite coating on aluminium to enhance surface and mechanical properties for automotive applications, J. of Adhe. Sci. Tech. **5** (2025) 2874. doi: https://doi.org/10.1080/01694243.2025.2573650
35. *Nayab*, *S., Baig*, *H.*, *Ghaffar*, *A.,Tuncel*, *E., Oluz*, *Z., Duran*, *H., Yameen*, *B.,* Silica based inorganic–organic hybrid materials for the adsorptive removal of chromium, RSC Adv. **8** (2018) 23963. doi: https://doi.org/10.1039/C8RA04209H
36. *Feng*, *S., Ni*, *J., Li*, *S., Cao*, *X., Gao*, *J., Zhang*, *W., Feng*, *S.,* Removal of hexavalent chromium by electrospun silicon dioxide nanofibers embedded with copper-based organic frameworks, Sustainability **14** (2022) 13780. doi: https://doi.org/10.3390/su142113780
37. *Raji*, *Z., Karim*, *A., Karam*, *A., Khalloufi*, *S.,* Adsorption of heavy metals: Mechanisms, kinetics, and applications of various adsorbents in wastewater remediation—a review, Waste **1** (2023) 775. doi: https://doi.org/10.3390/waste1030046
38. *Babel*, *S., Kurniawan*, *T. A.,* Low-cost adsorbents for heavy metals uptake from contaminated water: A review, J. Hazard. Mater. **97** (2003) 219. doi: https://doi.org/10.1016/S0304-3894(02)00263-7
39. *Mohan, D., Pittman Jr.*, *C. U.,* Activated carbons and low-cost adsorbents for remediation of tri- and hexavalent chromium from water, J. Hazard. Mater. **137** (2006) 762. doi: https://doi.org/10.1016/j.jhazmat.2006.06.060
40. *Alrowais*, *R., Bashir*, *M. T., Khan*, *A. A., Bashir*, *M., Abbas*, *I., Abdel Daiem*, *M. M.,* Adsorption and kinetics modelling for chromium (Cr^{6+}) uptake from contaminated water by quaternized date palm waste, Water **16** (2024) 294. doi: https://doi.org/10.3390/w16020294
41. *Alharissa*, *E. Z., Efhiliana*, *Y., Roto*, *R., Mudasir, M., Wahyuni*, *E. T.,* Efficient removal of Cr(VI) contaminant using recoverable silica from volcanic ash as natural adsorbent: Synthesis and activity in the mechanism and kinetic adsorption, Heliyon **10** (2024) e23273. doi: https://doi.org/10.1016/j.heliyon.2023.e23273
42. *Amanze*, *K., Amanze*, *J. O., Okore*, *G., Ngozi-Olehi*, *L. C., Okeke*, *P. I., Uchegbu*, *R. I., Eze*, *G. C.,* Pragmatic approach to the removal of Cu(II) ions from aqueous solution using silica: A kinetic, isothermal and thermodynamic study, J. Mater. Sci. Res. Rev. **8** (2025) 10. doi: https://doi.org/10.9734/jmsrr/2025/v8i2413
43. *Tatah*, *V. S., Otitoju*, *O., Ezeonu, C. S., Onwurah*, *I. N. E., Ibrahim*, *K. L. C.,* Characterization and adsorption isotherm studies of Cd(II) and Pb(II) ions bioremediation from aqueous solution using unmodified sorghum husk, J. Appl. Biotechnol. Bioeng. **2** (2017) 113. https://doi.org/10.15406/jabb.2017.02.00034
44. *Ali*, *I. H., Alrafai*, *H.,* Kinetic, isotherm and thermodynamic studies on biosorption of Cr(VI) by using activated carbon from leaves of *Ficus nitida*, Chem. Cent. J. **10** (2016) 36. doi: https://doi.org/10.1186/s13065-016-0180-1
45. *Foo*, *K. Y., Hameed*, *B. H.,* Insights into the modeling of adsorption isotherm systems, Chem. Eng. J. **156** (2010) 2. doi: https://doi.org/10.1016/j.cej.2009.09.013
46. *Adamu*, *A. A., Iyun*, *O. R. A., Habila*, *J. D.,* Adsorption and thermodynamic studies of the corrosion inhibition effect of *Desmodium adscendens* (Swartz) extract on carbon steel in 2 M HCl, BMC Chem. **19** (2025) 163. doi: https://doi.org/10.1186/s13065-025-01541-y
47. *Putz, A. M., Ciopec, M., Negrea, A., Grad, O., Ianăşi, C., Ivankov, O. I., Almásy, L.,* Comparison of structure and adsorption properties of mesoporous silica functionalized with aminopropyl groups by the co-condensation and post-grafting methods, Materials **14** (3) (2021) 628. doi: https://doi.org/10.3390/ma14030628
48. *Ianăşi, C., Ianăşi (b. Svera), P., Negrea, A., Ciopec, M., Ivankov, O. I., Kuklin, A. I., Almásy, L., Putz, A. M.,* Effects of catalysts on structural and adsorptive properties of iron oxide–silica nanocomposites, Korean J. Chem. Eng. **38** (2021) 292. doi: https://doi.org/10.1007/s11814-020-0675-2
49. *Jadhav, S. A., Garud, H. B., Thoravat, S. S., Patil, V. S., Shinde, P. S., Burungale, S. H., Patil, P. S.,* Synthesis and testing of functional mesoporous silica nanoparticles for removal of Cr(VI) ions from water, Biointerface Res. Appl. Chem. **11** (2021) 8599. http://doi.org/10.33263/BRIAC112.85998607
50. *Mehdinia, S. M., Moeinian, K., Rastgoo, T.,* Rice husk silica adsorbent for removal of hexavalent chromium pollution from aquatic solutions, Iranica J. Energy Environ. **5** (2) (2014) 64528. doi: https://doi.org/10.5829/idosi.ijee.2014.05.02.15
51. *Kandasamy, S., Meenachi, S., Kr, S. K., Thamaraikannan, V.,* Removal of chromium from tannery wastewater by rice husk ash nanosilica, Appl. Res. **2** (2023) 202200093. doi: https://doi.org/10.1002/appl.202200093
52. *Rodiah, S., Huljana, M., Al Jabbar, J. L., Ichsan, C., Marzuki, H.,* Silica rice husk as adsorbent of Cr(VI) ions prepared through sol–gel method, Walisongo J. Chem. **4** (2021) 65. doi: https://doi.org/10.21580/wjc.v4i1.8045